Technical Report No. 9

May 1966

INTRINSIC DEFECTS IN CdS

Contract: NSG-573
National Aeronautics and Space Administration
Goddard Space Flight Center
Greenbelt, Maryland

Principal Investigator: K. W. Böer
Department of Physics
University of Delaware
Newark, Deaaware

INTRINSIC DEFECTS IN CdS

by

Charles Alvah Kennedy

A thesis submitted to the Faculty of the University of Delaware in partial fulfillment of the requirements for the degree of Master of Science in Physics.

June, 1966

ACKNOWLEDGMENT

Available space, the forbearance of the reader and the self-respect of the author forbid listing all of the individuals, and their respective contributions, without whose influence this thesis would have remained unwritten. The author does, however, wish to express a very special thanks to Professor K. W. Böer for his tireless guidence and, as it seems in retrospect, his infinite patience.

ABSTRACT

Thermal defects, occuring in the temperature range between room temperature and 350°C, were "frozen-in" in cadmium sulfide single crystal platelets in ultra-high vacuo and the effects of the resulting disorder upon the spectral distribution of photoconductivity in the visible range and upon conductivity glow curves were studied. Parallel shifts toward higher conductivity with increasing heat treatment temperatures in both the spectral response curves and the glow curves are interpreted in terms of dissociation of a defect associate, composed of at least three point defects, which acts as a recombination centre.

Glow curves simultaneously show growth of peaks at approximately 200°K and 440°K, These peaks, it is felt, are due to the products of the dissociation. Both of these peaks are believed to be associated with cadmium vacancies- the former a V_{cd} and the latter a cluster corresponding to an S_n molecule.

By an annealing process, the crystals could be returned to approximately their pre-heat treated states.

350°C heat treatments resulted in a marked irreversible increase in the intrinsic photoconductivity and the dark current, a decrease and an increase in the 200°K and 440°K peaks respectively. These effects are believed to be related to the desorption from the crystal's surface of oxygen and to the formation of cadmium vacancy clusters (S_n molecules).

Author

TABLE OF CONTENTS

CHAPTER I

INTRODUCTION

It is well known that the photo-electrical properties of cadmium sulphide are strongly dependent on the defect structure of the crystal. The effects of many impurities in CdS have been studied extensively (1-6) and their properties are beginning to be understood. However, although a considerable amount of literature has appeared on the subject (5, 7-18), less progress has been made toward the understanding of intrinsic defects in CdS (i.e. defects composed of the native atoms themselves). One reason for this is that, whereas impurities can be incorporated into crystals in concentrations in excess of 10^{18} cm.$^{-3}$, most intrinsic defects are not found at room temperature in concentrations above 10^{15}cm.$^{-3}$ as can be seen from TSC curves and gain factor estimations-which is on the order of the concentrations of accidental impurities in "pure" crystals, Another difficulty arises from the fact that the variety of intrinsic defects (including associated point defects) present in the crystal under any given set of conditions can be large and experimental results usually do not afford a means of distinguishing between a given point defect and a defect associate involving this defect. As an example, the cadmium vacancy has to date been associated with at least five different energy levels in the forbidden gap ranging from a few tenths to 1.8 eV. from the conduction band edge (5, 13, 15, 18).

It is the purpose of this work to investigate the changes in intrinsic defect sturcture in undoped single crystal platelets of CdS resulting from heat treatments in vacuo in the temperature range between room temperature and

350°C by means of the spectral response of photoconductivity and conductivity "glow" curves and to make, in conjunction with other experiments, further contribution to the identification of the defects occuring in this temperature range.

CHAPTER II

THEORY

II-1. Intrinsic Defects in CdS (19-20)

All crystals contain imperfections. In addition to impurity atoms which are unavoidably introduced during the growth of the crystal, there are certain other point defects composed of the native atoms. Of these, the simplest are: (a) vacancies, (b) interstitials, and (c) substitutionals. In addition to single atom imperfections, there can occur (d) associates (clusters) of point defects. Let us consider some of these intrinsic defects in more detail.

II-1-1. The Schottky disorder involves the removal of an atom from its normal lattice site to some place on the crystal's surface leaving behind a vacancy. In a binary compound like CdS, one is required to impose a quasi neutrality condition on the formation of these defects. Since CdS is approximately 50% ionic (21), it is necessary to form an equal number of cadmium and sulfur vacancies since the removal from the crystal of N cadmium atoms would, for example, leave the crystal's interior negatively charged and its surface positively charged. Hence in order to preserve quasi charge neutrality, N sulfur atoms must also be removed and placed at the surface. In an otherwise perfect crystal, the formation of Schottky defects is then given by the equilibrium condition:

$$0 \rightleftharpoons V_{cd} + V_s \qquad (1)$$

where V_{cd} means a vacancy at a Cd site and V_s means a vacancy at a sulfur site. Application of the mass-action law gives:

$$[V_{cd}] \quad [V_s] = K_s \tag{2}$$

where the bracketed quantities are the concentrations and where K_s depends on the temperature. Hence it is seen from equation (2) that the product of the concentrations of Cd vacancies and S vacancies is a constant at a given temperature. Since we are bounded by the quasi-neutrality condition $[V_{cd}] = [V_s]$, we can write:

$$[V_{cd}] = [V_s] = K_s^{1/2} \tag{3}$$

By applying Boltzmann statistics it can be shown (22) that the density of cadmium or sulphur vacancies in thermal equilibrium with an otherwise perfect crystal at temperature T is given by:

$$[V_{cd}] = [V_s] = N_L e^{-E_s/2kT} \tag{4}$$

where N_L is the total density of lattice sites and E_s is the energy required to remove the atom from its lattice position and place it on the surface.*

In Appendix A it is shown that the formation of Schottky defects is probably not an important effect in the temperature range involved in this investigation (i.e. up to 350°C).

* If one takes into account that the creation of Schottky defects results in a change in entropy both for geometrical reasons and because of changes in the vibrational frequencies of the neighboring atoms, it can be shown (23) that the right hand side of equation should be multiplied by a factor γ_s which is believed to be on the order of 10^3 or 10^4.

II-1-2. The Frenkel defect involves the formation of a vacancy and an interstitial by removing an atom from its normal lattice site and placing it in an interstitial position. The Frenkel defect for cadmium* is characterized then by the relation:

$$Cd_{Cd} + V_I \rightleftharpoons V_{Cd} + Cd_I \tag{5}$$

where Cd_{Cd} means a Cd atom in a Cd site, V_I means a vacant interstitial position and Cd_I is a Cd atom in an interstitial position.

Application of the mass-action law to equation (5) yields:

$$\frac{[Cd_I]\ [V_{Cd}]}{[Cd_{Cd}]\ [V_I]} = K'_F \tag{6}$$

where K'_F is again dependent upon the temperature. For reasonably low degrees of disorder however.

$$[Cd_{Cd}] \cong [V_I] \simeq \text{const.}$$

Hence

$$[Cd_I]\ [V_{Cd}] = K_F \tag{7}$$

If it is assumed that essentially all of the cadmium interstitials and vacancies come from Frenkel type disorder we can write:

$$[Cd_I] = [V_{Cd}] = (K_F)^{1/2} \tag{8}$$

* Assuming single ionized Cd and S (the ionic radius of sulfur ions is roughly twice that of cadmium) we can neglect the formation of anti-Frenkel defects (sulfur).

Again one can apply Boltzmann statistics to Frenkel disorders and obtain

$$[Cd_I] = [V_{Cd}] = N_L e^{-E_F/2kT} \qquad (9)$$

where E_F is the energy required to remove the Cd atom from its lattice site and place it into an interstitial position.*

Böer, Boyn and Goede (24) have estimated that the energy of formation for Frenkel disorders may be as high as 3.2 eV and more recent studies (25) indicate that it may be even as high 7.3 eV. It is seen from Appendix A that such high energies result in negligible Frenkel disorder concentrations even at 350°C.

II-1-3. The substitutional disorder is one in which an atom of one type resides in a lattice site normally intended to house an atom of the other type. It should first be noted that it is felt that this disorder is less probable than Frenkel or Schottky disorders because a sulfur vacancy and a cadmium interstitial for example, have the same effective charge and hence they would tend to repel one another. If, however, substitutional disorders are found in CdS one would expect that Cd atoms in S sites would be more abundant than S atoms in Cd sites. There are two reasons for this. First, it is well known that CdS is slightly over stoichlometric in cadmium (26). In addition, the relative sizes of the Cd and S ions are such as to render a sulfur ion in a Cd site mechanically unstable

* As with the case of Schottky disorders, the right hand side of equation 9 should be corrected (23) for changes in the entropy by being multiplied by an appropriate factor γ_F which is suspected of being somewhat smaller than 10^3.

II-1-4. Defect associates are composed of aggregates of point defects which lie spatially close enough together to be subject to interaction. This interaction can change the properties of the component defects. Williams (27), for example, has shown that the association of a donor and an acceptor results in shifts in their respective energy levels. In addition, when a donor and an acceptor associate, the probability of electron transitions between their respective energy levels can increase serving to enhance the recombination of free electrons and holes (28).

With a random distribution of intrinsic defects there is a certain probability that some of these defects will occupy neighboring sites thus forming associates of two, three etc. point defects. With the presence of forces acting between these defects, the concentrations of various associates will be different (i.e. they will be larger if attractive forces are present and smaller if the forces are repulsive).

If one considers the case where two point defects D_1 and D_2 come together to form an associate with an enthalpy change ΔH, according to the relation

$$D_1 + D_2 \rightleftharpoons (D_1D_2) + \Delta H, \tag{10}$$

it can be shown (29) that for the case where only one type of associate is present (e.g. D_1 and D_2 nearest neighbors) and where the total number of point defects of each specie remains constant

$$\frac{[D_1]\ [D_2]}{[(D_1\ D_2)]} = \gamma_{12} e^{-\Delta H/kT} \tag{11}$$

where the brackets denote fractional concentrations and the factor γ_{12} depends upon the entropy change. Since only one

type of associate is present,

$$[(D_1\ D_2)] + [D_1] = [D_1]_{total}$$
$$[(D_1\ D_2)] + [D_2] = [D_2]_{total} \qquad (12)$$

letting $[D_2]_{total} = m\ [D_1]_{total}$, where m is some constant, and looking at the point at which half of the defects D_1 are associated, equation (11) becomes:

$$\ln \frac{m-1/2}{\gamma_{12}} + \ln [D_1]_{total} = -\frac{\Delta H}{kT}_{0.5} \qquad (13)$$

Clearly then, the point at which half of the defects D_1 are are associated shifts to higher temperatures as $[D_1]_{total}$ increases.

The variation of the free and associated concentrations with temperature can be seen by considering their behavior at high and low temperatures. Consider for simplicity the case for which m=1 (i.e. where $[D_1]_{total} = [D_2]_{total} \equiv [D]$. At high temperatures most of the imperfections are dissociated and equations (12) can be written.

$$[D_1] = [D_2] = [D] \qquad (14)$$

Under this condition equation (11) becomes

$$\ln [(D_1D_2)] = 2 \ln [D] - \ln \gamma_{12} + \frac{\Delta H}{kT} \qquad (15)$$

The logarithm of the associate concentration increases linearly with increasing 1/T.

At low temperatures, association is essentially complete. Hence.

$$[(D_1D_2)] = [D] \qquad (16)$$

This yields:

$$\ln [D_1] = \ln [D_2] = \frac{1}{2} (\ln[D] + \ln \nu_{12} - \frac{\Delta H}{kT} \qquad (17)$$

In this case, the logarithm of the concentration of free defects decreases linearly with increasing 1/T but with half the slope of the previous case.

Several authors have already explained experimental results in terms of native defect associates. Niekisch (18) has attributed a trapping level lying 0.22 eV below the conduction band to an associate of two sulfur vacancies and a centre lying somewhere between 0.8 and 1.8 eV to a $V_{Cd}V_s$ complex. Nicholas and Woods (7) have suggested that a trapping level lying 0.83 eV below the conduction band is due to a complex aggregate of point defects. Woods (5) and Skarman (13) have attributed a trapping level which gives rise to a TSC peak between 330°K and 340°K to a $V_{Cd}V_s$ associate.

One possible force between defects arises from the partially ionic bonding of CdS. One expects, for example, that, because of the Coulomb interaction, a sulfur vacancy and a cadmium vacancy-having a positive and a negative charge respectively-would associate with some facility whereas two cadmium vacancies or two sulfur vacancies would have to overcome a repulsive force in order to associate. In accordance with this force the possible pairs of native defects in CdS are listed in Table I where they are qualitatively classified according to their electrical and geometrical stability. The criteria for this classification are based on a model of singly ionized atoms. Because of the large size of the sulfur interstitial, any associate involving it will fall into the geometrically unstable category.

Elect. Stable Geom. Stable	Elect. Unstab. Geom. Stable	Elect. Stable Geom. Unstab.	Elect. Unstab. Geom. Unstab.
V_{Cd} V_s	$V_{Cd}V_{Cd}$	S_I V_s	S_I V_{Cd}
Cd_I V_{Cd}	V_s V_s	Cd_I S_I	Cd_I Cd_I
	Cd_I V_s		S_I S_I

TABLE I

Double Defect Associates in CdS

Another driving force for the formation of stable associates arises from the binding energies of various molecular species of cadmium and sulfur. In figure 1 are shown the binding energies in eV per atom as a function of the number of atoms per molecule for sulfur (30) and cadmium.*

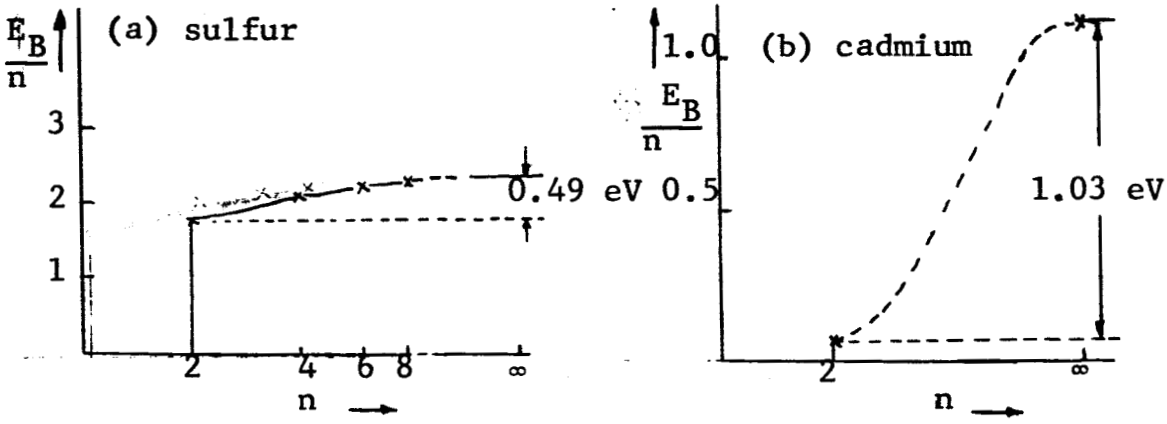

Fig. 1. Binding energies (in eV per atom) in species X_n for: (a) sulfur; (b) cadmium.

* The only two molecular species of cadmium for which the binding energies are known are Cd_2 (0.087eV(31)) and Cd_∞(the cohesive energy (32)). Intermediate associates presumably have intermediate binding energies per atom.

For sulfur (figure 1a), there is a large binding energy for S_2. Hence one might expect in CdS clusters of two sulfur atoms. In addition, however, the binding energy per atom of the larger sulfur molecules (S_4, S_6 and S_8) is significantly larger and therefore one expects that these intermediate associates (corresponding to clusters of cadmium vacancies) are also probably found in CdS.

With cadmium (figure 1b) the situation is somewhat different. The binding energy for Cd_2 is very small thus serving as an indication that the Cd_2 cluster is not a very stable associate and therefore will not be found in any appreciable concentration at room temperature. A considerably larger energy, however, is gained by condensing Cd to form a metal. Hence, by this arguement, one expects cadmium clusters large enough to form colloidal particles - or equivalently, one expects larger clusters of sulfur vacancies.

In order for defect clusters to dissociate it is necessary that the products of dissociation separate via some diffusion process. Since clusters of defects, due to their size, cannot diffuse with the facility of single point defects, it seems reasonable to assume that dissociation takes place by the removal of single point defects rather than by the separation of the associate into two or more subclusters. For example, a cluster of four sulfur vacancies would probably dissociate at lower temperatures by the transformation

$$V_{s_4} \rightarrow V_{s_3} + V_{s_1}$$

or even by

$$V_{s_4} \rightarrow V_{s_2} + 2V_{s_1}$$

rather than by

$$V_{s_4} \rightarrow 2V_{s_2}$$

because the V_{s2} clusters cannot readily diffuse. As a consequence of these arguments, it seems possible that the dissociation of defect associates may well be a source of single point defects which, due to the lower binding energies involved, is operative at lower temperatures than either the Frenkel or Schottky mechanism.

II-2. Levels in the Forbidden Gap.

It is well known that the presence of native defects and impurities in a semiconducting or insulating crystal in general give rise to localized electron energy levels which lie in the band gap (33). For the discussion of photo-electrical properties of the crystal, these levels can be divided into three groups (34, 35): electron traps, hole traps and recombination centres. An electron trap is defined as an energy level at which an electron has a higher probability of being thermally excited into the conduction band than of falling into a hole in the valence band. Similarly, a hole trap is a level at which a captured hole has a higher probability of being thermally excited into the valence band than of meeting a conduction electron. A recombination centre is then a level at which recombination is more probable.

The distinction between these groups of levels can be made by considering the demarcation levels, D_n and D_p, (figure 2) defined by Rose (35) in the following manner. Consider a distribution of energy levels all of the same class - i.e. all having the same capture cross sections for electrons S_n and the same capture cross sections for holes S_p. S_n and S_p may be different. The demarcation level for electrons D_n for this class of levels is defined as a value of energy at which, if there is an electron, the electron has an equal probability of being thermally driven into the conduction band and of falling into a hole in the valence band. The

hole demarcation line D_p is similarly a value of energy at which, if there exists an energy level, holes suffer an equal probability of being thermally driven into the valence band and of participating in recombination. Clearly then, for this class of levels, electron traps then lie between E_c and D_n and hole traps between D_p and eV and the recombination centres are those levels which lie between D_n and D_p.

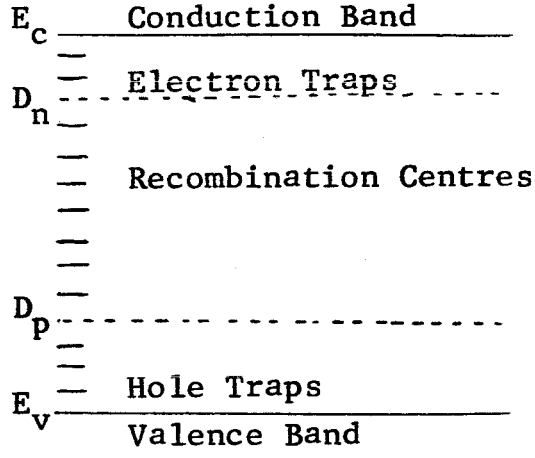

Figure 3.

It can be shown (35) that the demarcation levels obey the relations

$$E_c - D_n = E_c - E_{fn} + kT \ln \frac{nS_n}{pS_p} \qquad (18)$$

$$D_p - E_v = E_{fp} - E_v - kT \ln \frac{nS_n}{pS_p}$$

where E_{fn} and E_{fp} are the quasi-Fermi levels, for electrons and holes respectively, defined by:

$$n = N_c(T) \exp - \frac{E_c - E_{fn}}{kT} \qquad (19)$$

$$p = N_v(T) \exp - \frac{E_{fp} - E_v}{kT}$$

where $N_c(T)$ and $N_v(T)$ are the effective densities of states in the conduction and valence bands respectively and are functions of temperature and the effective mass.

Equations (18) reveal that, to a first approximation, (for nS_n within a few orders of magnetude of pS_p and $T \leq$ room temperature) the demarcation levels lie very close to the quasi-Fermi levels.* Hence one can often think of electron traps as those levels occuring between E_c and E_{fn}, hole traps as those lying between E_{fp} and E_v and recombination centres as being the levels between the quasi-Fermi levels. As a consequence, it is seen that by changing the free carrier concentrations - perhaps by changing the light intensity in the case of a photoconductor - it is possible to alter the relative densities of recombination centres and trapping levels. For instance an increase in light intensity would increase n and p thus spreading the quasi-Fermi levels and essentially converting any energy levels over which they have passed from traps into recombination centres.

There are several reasons to believe that the level distribution near the crystal's surface is different from that in the bulk. For one thing, the periodic potential of the lattice ceases to exist of the surface. According to Tamm (36), this interuption in periodicity alone can introduce levels in the forbidden zone. In addition, there are always present layers of adsorbed impurity atoms obtained from the surrounding atmosphere which can combine chemically with the host atoms to form entirely different compounds, such as CdO for example, near the surface. Still another source of surface states is the fact that many of the host

* For a given temperature and given free electron and hole concentrations, the quasi-Fermi levels are fixed. It is clear from equations (18) that there are as many sets of demarcation levels (D_{ni}, D_{pi}) as there are classes of levels (S_{ni}, S_{pi}) present in the crystal.

atoms are misplaced at the crystal's surface resulting in considerable disorder there. Bardeen (37) has treated the case where the number of surface states is comparable with the number of surface atoms and has pointed out that, depending on the state of occupancy of these levels, there can be a boundary layer between the surface and the bulk due to charging of the surface. Because of these arguments, one has little reason to expect that the photo-electrical properties of the surface are similar to those of the crystal's interior and, until more quantitative work in the field of surface studies has been done, one cannot completely rule out the surface as a source of certain experimental results.

II-3 Spectral Response of Photoconductivity and Conductivity Glow Curves.

There exist many experimental methods by means of which one can investigate the level distribution in the forbidden gap. Examples include luminescence, absorption studies, rise and decay times of photoresponse, methods of alternating light excitation, infrared and thermal quenching of photocurrents, spectral response of photoconductivity and the so-called conductivity "glow" curves. Of these methods, among the most economical-in terms of experimental facility versus information yield-are the last two. It is primarily for this reason that these two experimental approaches were used in this investigation.

II-3-1. The spectral response of photoconductivity in CdS is often discussed in terms of extrinsic photoconductivity or intrinsic photoconductivity depending on whether the wavelength of the exciting light used corresponds respectively to less or more energy than that of the band gap (2.4 eV at room temperature).

In the extrinsic range, the photon induced electron transitions which result in photoconductivity take place primarily between levels in the forbidden gap and the conduction band. Figure 3 shows the approximate range of extrinsic transitions covered by the spectral response curves obtained in this investigation. One can obtain from the extrinsic spectral response information about changes in the free carrier lifetime. This is indicated by a parallel shift to higher or lower photoconductivity of the entire extrinsic portion of the curve. In addition, however, one can obtain information about the changes in the level distribution in the covered range as indicated by the appearance or disappearance of peaks in the extrinsic spectral response.

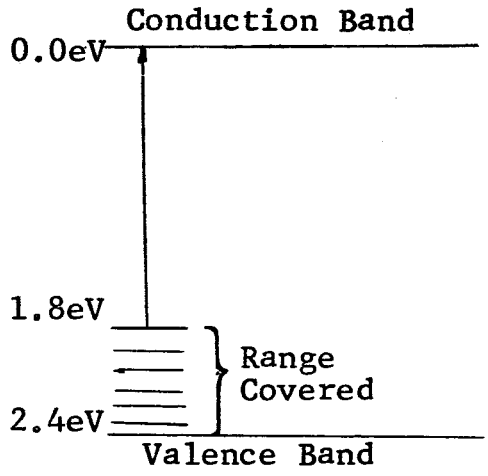

Figure 3.

In order to appreciate the relavency of intrinsic excitation to the investigation of level distributions it is necessary to appeal to absorption studies of CdS. Dutton (38) has investigated the absorption of visible light in "clean" CdS single crystals with the result that the absorption coefficient for $\lambda<500$ mμ is approximately $10^{5}cm^{-1}$ while for $\lambda>520$ mμ it is less than 1 cm^{-1} at room temperature. This means that for $\lambda<500$ mμ the intensity of the transmitted light has dropped to 1/e its value at the surface within 10^{-5}cm. of the surface leaving a major part of the crystal's bulk in the dark. Since the mean free path for conduction electrons at room temperature is 10^{-6}cm. (Appendix B), many of the electrons liberated with intrinsic light have an opportunity to collide with surface imperfections. As a

consequence, the resulting electral measurements are probably strongly affected by the surface properties of the crystal and changes in the intrinsic spectral response can be used as a measure of changes in these surface properties.

II-3-2. Conductivity glow curves* are useful in obtaining information about electron traps in CdS. They derive their strength as an analytic tool from the fact that electron traps which are filled with electrons at one temperature will empty their electrons into the conduction band at some higher temperature where their presence will be seen as a transient increase in conductivity. Experimentally, this is effected in the following manner. The crystal is cooled to a low temperature and irradiated with light. This serves the purpose of filling many of the traps (i.e. the electron quasi-Fermi level is moved closer to the conduction band). Having filled these traps, the exciting light is removed and the crystal is heated in the dark at a uniform rate. A plot of conductivity versus temperature can exhibit peaks provided the heating rate is not too slow (39). From the temperature at which a peak is seen one can obtain an estimate of the energetic location of the trap, as discussed below, and the area beneath the peak provides one with the density of the trap as shown in Appendix C.

In principle, one glow curve provides enough information to determine the trapping spectrum over which the electron quasi-Fermi level has passed during heating. In practice, the analysis of the data can be quite complicated. Many theoretical methods have been suggested (39-51) for

---

* In the literature these are sometimes referred to as thermally stimulated currents (TSC) or thermally induced currents (TIC).

dealing with the data, most of which discuss a model, Figure 4; involving a single group of traps lying at an energy ΔE below the conduction band having a thermal emptying probability characterized by

$$\alpha = \alpha^* \exp^{-\Delta E/kT}$$

where α^* is the so-called attempt to escape frequency. In addition these traps have a filling mechanism governed by

$$\beta = S_t v_{th}$$

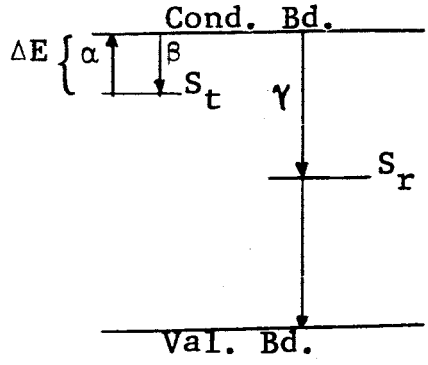

Figure 4.

where S_t is the capture cross-section for electrons and v_{th} is the thermal velocity of conduction electrons. The simplest models also include some recombination process governed by

$$\gamma = S_r v_{th}$$

where S_r is the capture cross-section for electrons of the recombination centre. The relative magnetudes of the capture cross-sections S_t and S_r are important. For example, if S_t is much smaller than S_r no appreciable retrapping of electrons will occur and hence once an electron is freed from the trap it will contribute but once to the conductivity after which it will fall into a recombination centre and recombine with a hole. If, on the other hand, S_t is much larger than S_r, fast retrapping occurs and the electron may well contribute to the conductivity more than once. As a result of this, glow curve theories often represent one of three special cases: (a) $S_t \ll S_r$ (monomolecular recombination), (b) $S_t \simeq S_r$, (c) $S_t \gg S_r$ (fast retrapping).

One of the first theories of glow curves was proposed by Randall and Wilkins (40) which involved the simplifying assumption that $\beta = 0$. The result was a semi-

empiracl expression for trap depth in terms of the temperature T_m of the glow peak:

$$\Delta E = 25\ kT_m \qquad (20)$$

Later theoretical investigations of Böer, Oberländer and Voigt (39) showed, on a more rigorous basis, that not only is equation (20) satisfactory for $\beta = 0$, but also the Randall-Wilkins result can be often used to find trap depths to within $\pm$ 4 k T_m even when fast retrapping occurs.

It is well known (52) that the position of the glow maximum is somewhat dependent upon the heating rate in a fashion such that higher heating rates correspond to higher temperatures of the glow peak. However, above the critical heating rate, over a range of heating rates from 0.1 to 1.0C^o per sec., the deviation of the current maximum has been shown to be less than 6% in copper doped and cobalt doped CdS (39).

As a consequence of these considerations, the Randall-Wilkins result is felt to give reasonably adequate estimations of the trap locations and hence it will be used here.

CHAPTER III

EXPERIMENTAL

III-1. Description of Equipment

The vacuum system (Figure 5) is composed of an all stainless steel tank, approximately 25 liters in volume, provided with Varian con-flat flanges containing electrical and mechanical feedthroughs and two glass viewing ports. Upon assembly, the system was thoroughly cleaned in accordance with the procedure recommended by Varian (Appendix D). The pumping system includes a Varian Vac-Sorb forepump, model #941-5610, by means of which a vacuum of 5×10^{-3} torr can be reached, and a Varian 125 liter per second Vac-Ion pump, model #911-5417, which, after discontinuing fore pumping by sealing off the system from the forepump, could be started and, with baking, produced vacua below 10^{-10} torr. The Vac-Ion pump could be baked out with the accompanying Varian Internal Heater, model #924-0029. The pressure in the region of the crystal was measured by means of a Varian ionization gauge, model #971-0003,

The crystal holder (figures 5 and 6) is a copper block which can be heated or cooled from the outside of the vacuum system. Light transmitted by the crystal passes through a hole in the copper block and into the photocell, RCA 926. This affords a means of controlling the light intensity. The crystal holder is completely surrounded by a copper cup which is in thermal contact with the copper block. The function of the cup is to expose the crystal to a heat source (or sink) on all sides when it is being heated (or cooled) so as to minimize temperature gradients.

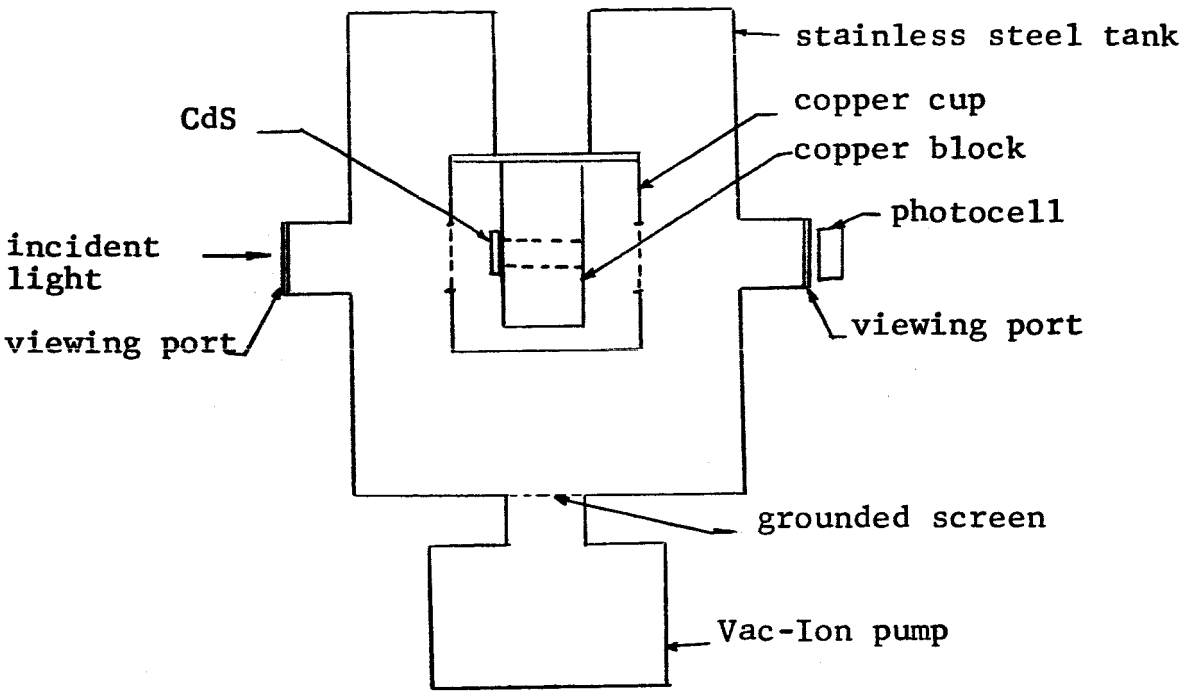

Figure 5. The Vacuum System

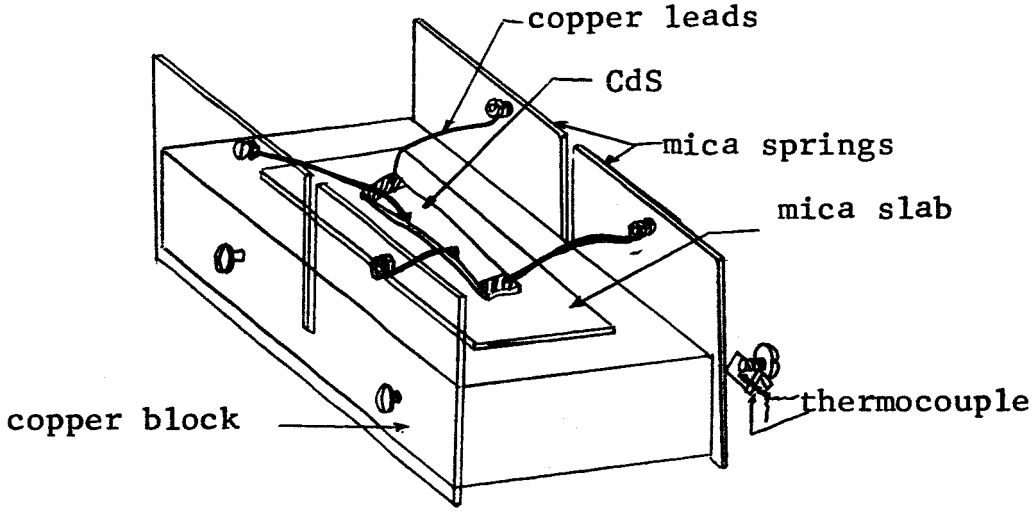

Figure 6. Crystal Mounting

in the crystal. This is necessary to assure homogeneous trap emptying in the case of TSC curves and to eliminate disturbances from the Seebeck effect. In the side of the copper cup are two holes which allow the incident light to fall upon the crystal and the transmitted light to pass to the photocell. These can be covered by means of copper shutters (not shown) which are operated by a Varian ultra-high vacuum rotary feed-through, #954-0026.

Another purpose served by the copper cup, shutters and grounded screen (Figure 5) is that they shield the crystal from bombardment by ions in the residual gas in the vacuum system which are formed when the Vac-Ion pump is in the glow discharge stage of pumping (at pressures higher than 10^{-4} Torr). This transient stage, lasting approximately one minute, is passed through during pumpdown.

The crystal platelet (of approximate dimensions 10mm. x 5mm. x 0.05mm.) is mounted on a thin slab of high resistivity (10^{14} ohm-cm) mica which lies on the copper block. The crystal is held in place by the pressure of the mica springs. The copper leads are sufficiently thick so as not to bend under the tension of the mica springs at elevated temperatures.

The temperature of the crystal was measured via two copper-constantan thermocouples in conjunction with a Minniapolis-Honeywell Rubicon potentiometer model #2745. These thermocouples were located at two different places on the copper block and were separated from the block by a piece of mica equal in thickness to that upon which the crystal lay. Preliminary tests showed the thermocouples to read within $1C^{o}$ of each other over a wide range of temperatures hence indicating that the heating was homogeneous over the block and that the crystal temperature was very

nearly that of thermocouples.

Figure 7 is a schematic diagram of the optical and electrical measurements system. Monochromatic light in the visible range was provided by a Bausch and Lomb grating monochromator #33-86-25-02 with accompanying tungsten light source #33-86-37-01. The spectral purity as specified by the manufacturer is approximately half intensity attenuation at $\pm$ 5 millimicrons for the slit settings used: input 1.35mm, output 0.75mm. The output of the monochromator in photons per second as a function of wavelength is shown in Figure 8 (curve #1). This was calculated from data furnished by the manufacturer on the total energy output as a function of wavelength. The number of photons per $cm.^2$-sec. incident upon the crystal was determined experimentally and the results are shown in figure 8 (curve #2).

An electric motor was attached to the monochromator by means of which the visible spectrum could be scanned at a rate of 20 mμ per hour from long to short wavelengths. The spectrum was scanned from long to short wavelengths because, for the crystals used in this experiment, the rise time of photoconductivity was much shorter than the decay time at room temperature. Since, as noted in section II-3-1, the absorption coefficient of CdS is considerably higher in the short wavelength region than in the long wavelength region, one can achieve steady state photocurrents more rapidly by sweeping in the direction of increasing absorption.

The current through the crystal was measured by means of a Keithley 413-A log scale micro-microammeter. The accuracy as specified by the manufacturer is within $\pm$ 0.2 decade.

In order to obtain an accurate measurement of the conductance of the bulk of the crystal - i.e. to eliminate

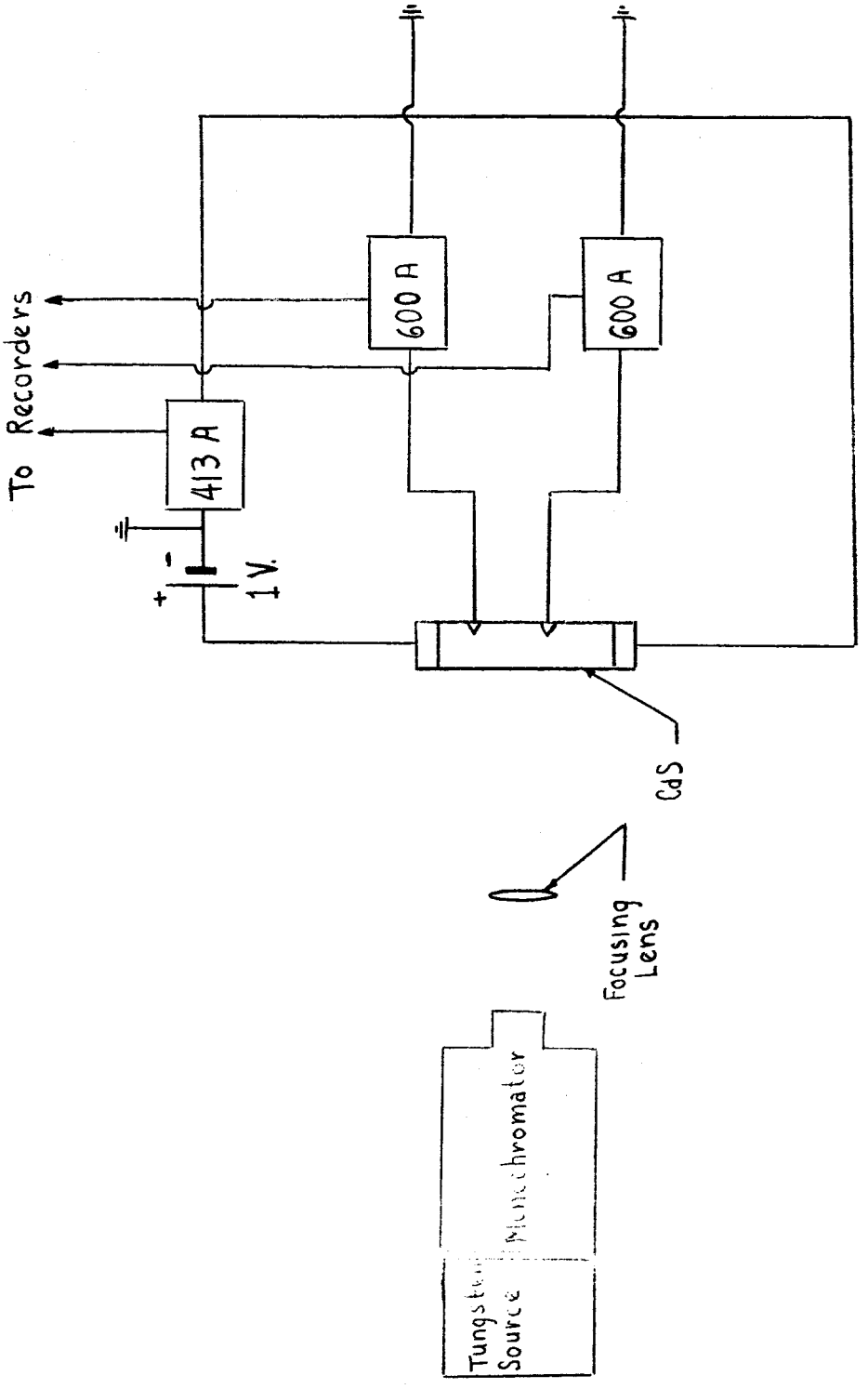

Figure 7. Optical and Electrical Measurements System

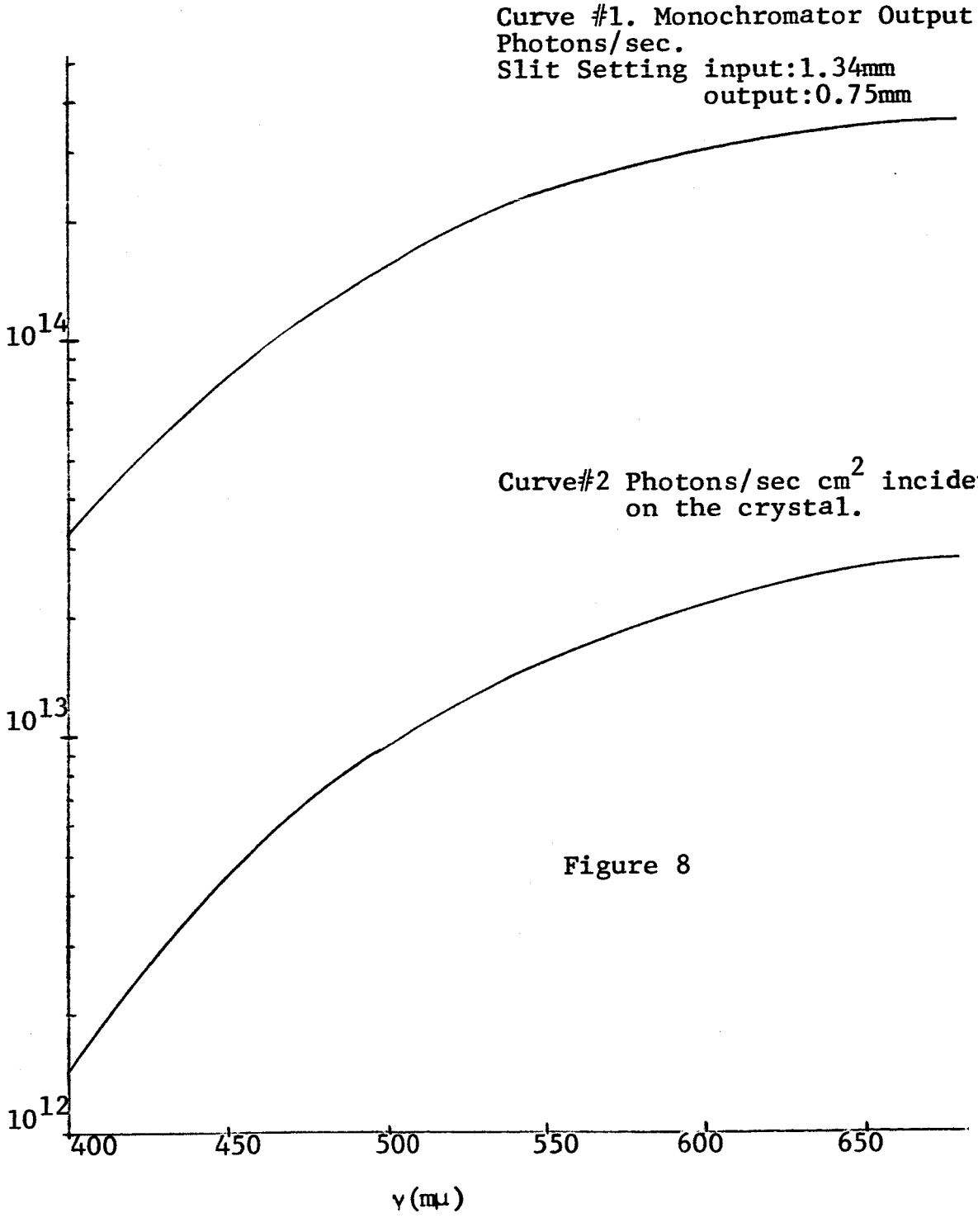
Curve #1. Monochromator Output
Photons/sec.
Slit Setting input:1.34mm
output:0.75mm
Curve#2 Photons/sec cm^2 incident
on the crystal.
10^{14}
10^{13}
10^{12}
400
450
500
550
600
650
γ(mμ)

Figure 8

the effects of barrier layers (53) at the current electrodes a four electrode method was used. The voltages at the two inner electrodes were probed by means of two Keithley 600-A electrometers which have an internal resistance of 10^{14} ohms and accuracy to within 2% full scale.

The electrodes were evaporated onto the unheated crystal in vacuo below 10^{-6} torr. Crystal #1 wore gold electrodes. Gold, although it does not make an ohmic contact with CdS, was used because of its ability to withstand high temperatures without changing its properties and because gold does not readily diffuse into CdS. Crystal #2 wore gold-chromium electrodes. The chromium was added in an attempt to increase the mechanical stability of the electrodes against being scratched by the copper leades as they expand and contract during heating and cooling.

The current through the crystal and the two probed voltages were continuously monitored by three Leads & Northrup Speedomax H chart recorders. These were calibrated so as to agree within 1% with the scale readings of the respective instruments driving them.

All electrical leads were shielded cables with the shielding grounded.

In addition to the two crystals reported on here, several other crystals have been investigated.

III-2 Experimental Procedure

As was indicated in the preceeding section, in order to attain a vacuum of 10^{-10} torr the system must be baked out. Without baking the pressure does not drop below 10^{-8} torr. The bakeout temperature is increased in such a way as to keep the pressure in the system well below 10^{-5} torr in

order to avoid gas discharge in the vacuum system. Ultimately a temperature of 350°C is reached both in the walls of the vacuum system and in the crystal and this temperature is maintained for several hours. In addition to outgasing the vacuum system, baking out at 350°C serves the purpose of destroying the virginity of the crystal. It is well known that CdS crystals in the virginal state often exhibit a very different photoconductive behavior than they do in subsequent experiments. Since it is not the purpose of this experiment to study the transition from virginal to heat treated states, but rather to study the effects of further heat treatments on heat treated crystals, it is of benefit to annihilate as much of the history (i.e. surface impurities etc.) of the particular crystal as possible. This is accomplished during bakeout.

The heat treatment cycle consists of the following steps, Following the 350°C bakeout, the crystal is annealed from 350°C to room temperature in a prescribed fashion. Figure 9 is a plot of temperature versus time for the annealing process. This particular curve was chosen because initial experiments indicated a noticeable change in defect structure occuring between 150°C and 200°C heat treatments. Hence much of the annealing time was spent in this region.

After annealing, a spectral response curve is obtained at room temperature. Following the spectral response measurement, the crystal is irradiated with 510 mμ light for a period of 30 minutes at room temperature. The crystal is then cooled to liquid nitrogen temperature and irradiation is continued there for 20 min. The reason for irradiating the crystal while it is still at room temperature is that it has been found (54) that in CdS there are certain traps which will not be filled if the crystal is irradiated only at liquid nitrogen temperature. This is due, it is suspected,

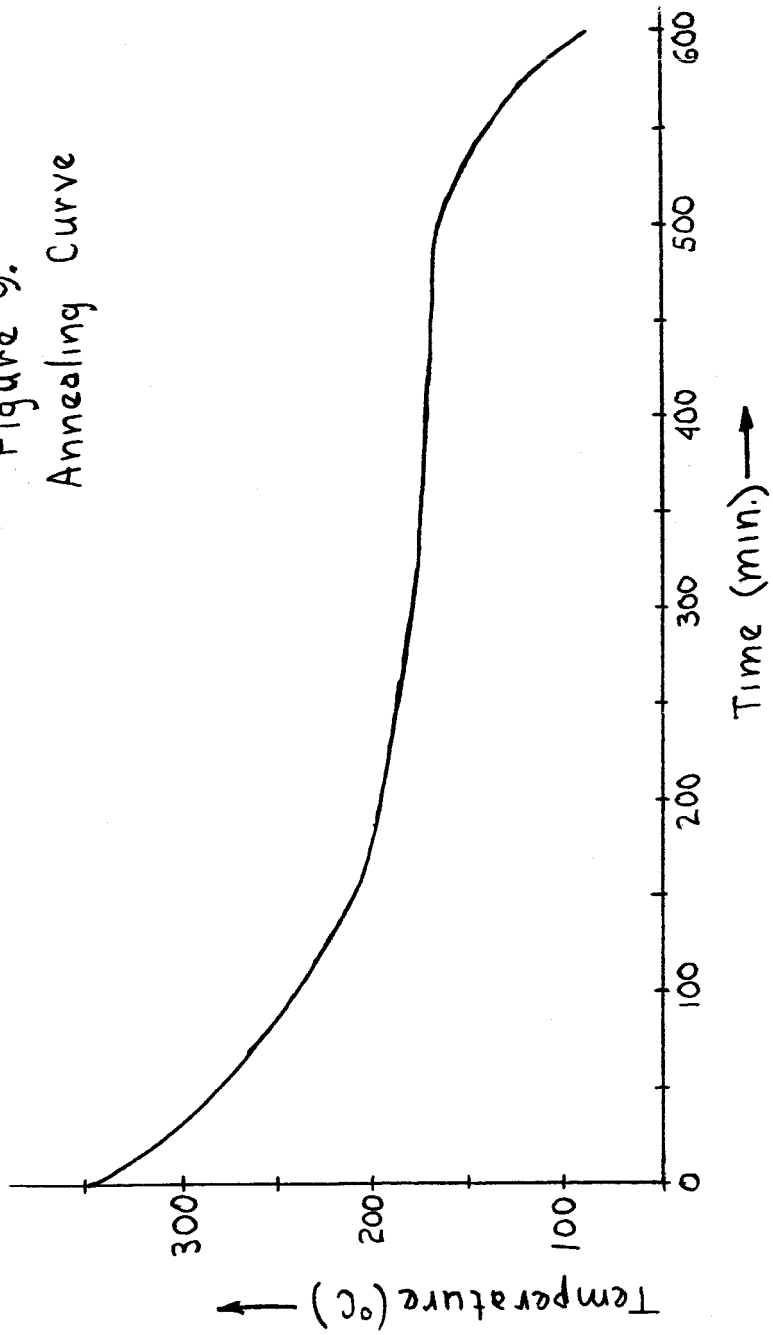

Figure 9.
Annealing Curve

to the presence of a repulsive potential barrier around these traps which the electron, at liquid nitrogen temperature, does not have sufficient energy to surmount. Immediately after the 50 minute trap filling, the light is switched off and a conductivity glow curve is run at a heating rate of 0.32 centigrade degrees per second up to 100°C. During this time the current and voltages are continuously monitored.

The crystal temperature is then held at 100°C. for one hour to instill equilibrium in the thermal defect subsystem. The crystal is then rapidly (at a rate of 1.2C°/sec.) cooled to room temperature. The rapid cooling is intended to freeze in the disorder incurred during the 100°C heat treatment. Following this freezing-in, a room temperature spectral response and a glow curve are obtained - the TSC curve going to 150°C.

Once at 150°C, the crystal is heat treated for one hour and rapidly cooled to room temperature. This is followed by a spectral response measurement and a glow curve to 200°C.

This pattern is repeated with heat treatment temperatures increasing in 50°C steps until finally a spectral response curve and a TSC curve are obtained after a 350°C heat treatment.

The crystal is then annealed as stated above and the entire cycle is repeated in order to verify reproducibility.

Two more cycles are run which differ from those described above only in that the light used to fill the traps for the glow curves is weakly absorbed extrinsic light of 650mμ wavelength as opposed to the strongly absorbed 510mμ light.

Finally the initial program with 510mμ trap filling is repeated as an additional check on the long term effects of heat treatments.

CHAPTER IV

EXPERIMENTAL RESULTS

Seven heat treatment-annealing cycles, as described in Chapter III, were run on crystal #1 and three on crystal #2.* There was considerable reproducibility in the results of these cycles. In section IV-1, the results of representative cycles are given. In section IV-2, changes in the spectral response curves and TSC curves for crystal #1 which took place over a period of 8 months (during which the pressure never rose above 5×10^{-10} torr) are given.

The data is presented in terms of current rather than conductance because occasionally the voltage difference between the two inner electrodes was too small to be accurately measured. It is felt, however, that this does not subtract significantly from the validity of the results since the appearance of and trends in the conductance curves, when they could be accurately measured, closely resembled those of the current curves. The points are replotted from curves obtained on the recorders and represent less than 20% error.

For the sake of brevity the curves are referred to by the heat treatment temperature after which they were obtained. For example the 300°C spectral response (or glow) curve obtained after heat treatment at 300°C.

IV-1 Representative Cycles.

IV-1-1. The spectral response curves obtained from three typical cycles are shown in figures 10, 11 and 12.

*A limiting factor for the number of experiments per crystal was the durability of the electrodes. Thermal expansion and contraction of the wires contacting these electrodes caused them to be scratched away resulting in poor contacts.

Figure 10 is for crystal #1 and figures 11 and 12 for crystal #2. It was observed in both crystals, and in others not reported on here, that the photocurrent suffered essentially a parallel shift toward higher currents with increasing heat treatment temperature without the appearance of any new peaks in the extrinsic range. It is also seen from the figures that the increase in the photocurrent was more pronounced in the region of extrinsic excitation than in the intrinsic range. The exception to this is found in crystal #1 where, upon heat treating at 350°C, the increase in intrinsic photocurrent was notably greater than the extrinsic increase in all of the seven cycles to which this crystal was subjected. The annealing process used here failed to reverse this intrinsic increase.

Heat treatments at 100°C produced no appreciable change in the experimental results and hence room temperature and 100°C curves are shown as one.

IV-1-2. Figures 13, 14 and 15 are the glow curves obtained for the three cycles respectively whose spectral responses are given above. Figures 13 and 14 are 510 mμ filled glow curves for crystals #1 and #2 respectively. Figure 15 is a set of 650 mμ filled glow curves for crystal #2. The trap densities have been calculated using the results of the analysis in Appendix C and are listed in Table II. All of these glow curves exhibit a parallel shift toward higher currents with increasing heat treatment temperature.

Crystal #1 (figure 13) shows two broad current maxima at approximately 200°K and 440°K. These were very insensitive to filling wavelength in that the 650 mμ filled glow curves exhibited exactly the same structure and changes as the 510 mμ filled ones. Up to 300°C heat treatments,

there appeared in this crystal very small, if any, growth of peaks. However, upon heating at 350°C, crystal #1 showed a decrease in the 200°K peak and an increase in the 440°K peak.

In crystal #2, a parallel shift is quite apparent in the 510 mμ filled glow curves (figure 14). In addition, however, there appears to be a pronounced growth of the broad peak at approximately 200°K. This effect was reproducible in crystal #2 (i.e. this peak could be annealed out and regrown by heat treating) but was not observed in crystal #1. Quite apparant in these glow curves are two peaks at 350°K and 385°K. These two peaks exhibit no noticeable growth. Growth of the peak at 440°K becomes evident after 300°C heat treatment. After 350°C heat treatment the 385°K and 440°K peaks are seen as one peak at 400°K.

Another interesting property of crystal #2 was that it showed considerable sensitivity to the filling wavelength. In figure 15 one can see the aforementioned parallel shift and some growth of the peak at approximately 200°K. Noticeably absent however, for 650 mμ filling, are the peaks at 350°K and 385°K.

IV-2. Changes Over Several Cycles

IV-2-1. Figure 16 shows the changes which occured in the spectral response curves for crystal #1 over an 8 month period during which the crystal was kept in vacuo below 5×10^{-10} torr and subjected to 7 cycles. This means that the crystal spent a total of approximately 16 hrs. at 350°C and roughly the same amount of time at 300°C, 250°C, etc. The changes are characterized by an increase in intrinsic photocurrent while the extrinsic photocurrent is virtually unaffected. This "irreversible" change occurred upon heat treating the crystal at 350°C. The 350°C curve was arbitrarily

chosen to represent this change in shape of the spectral response from cycle to cycle.

It was also noticed in crystal #1 that, over the course of these cycles, the dark current rose by approximately two orders of magnetude (i.e. from $\sim 10^{-11}$ to $\sim 10^{-9}$).

IV-2-2, Figure 17 is representative of the change in glow curves over the above mentioned period. Here too the 350°C curve was chosen as the representative. One observes here a reduction in the 200°K peak and an increase in the 440°K peak. This "irreversible" change was also a result of 350°C heat treatments. A similar trend was very slightly noticeable in crystal #2.

Investigations presently being made have thus far shown that CdS crystals heat treated at 1000°K in sulfur vapor (1000 torr) for several hours exhibit TSC behavior very similar to that of later cycles in figure 17 (i.e. one pronounced peak at 440°K).

Figure 10.
Spectral Response
for Crystal #1

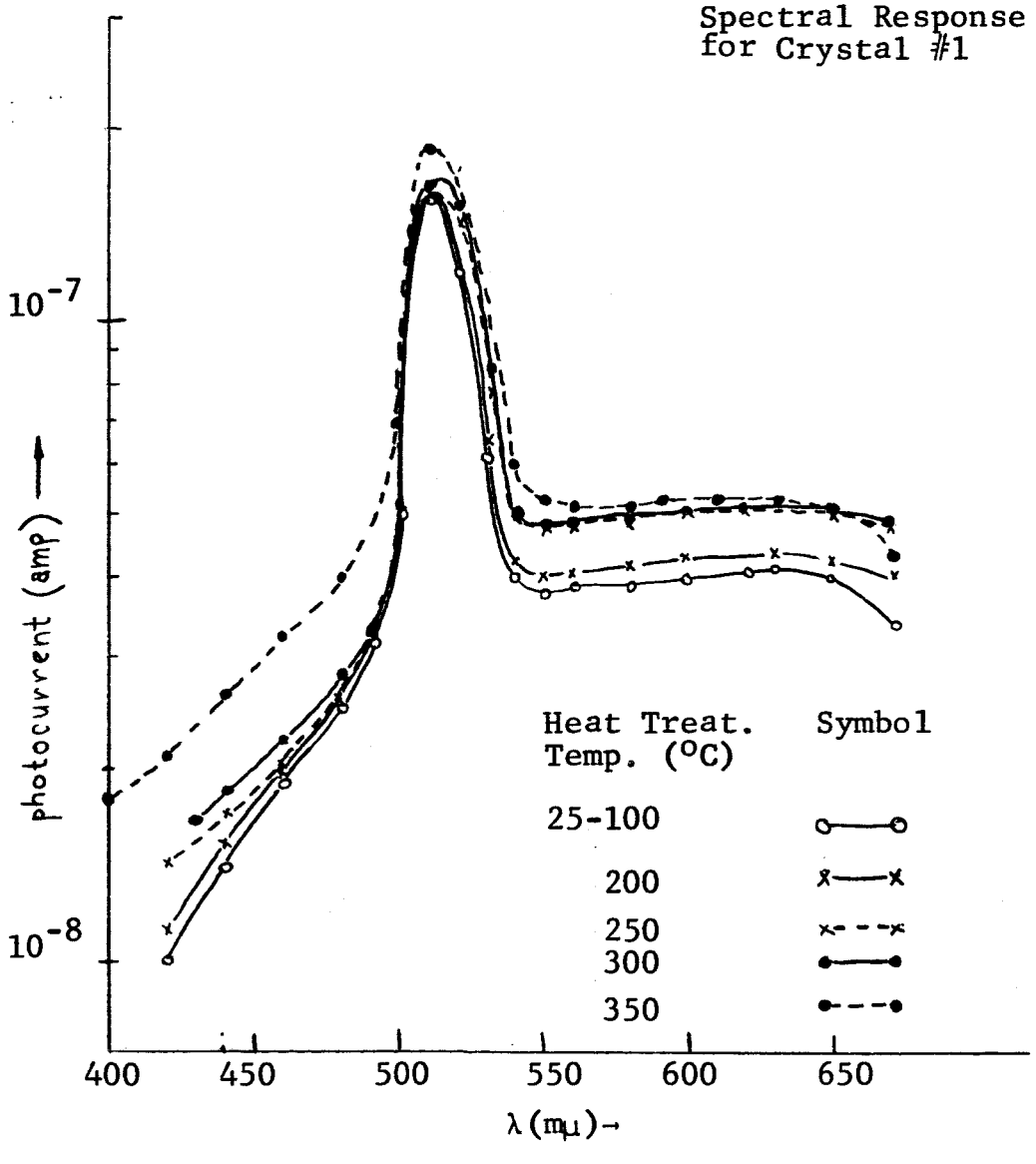

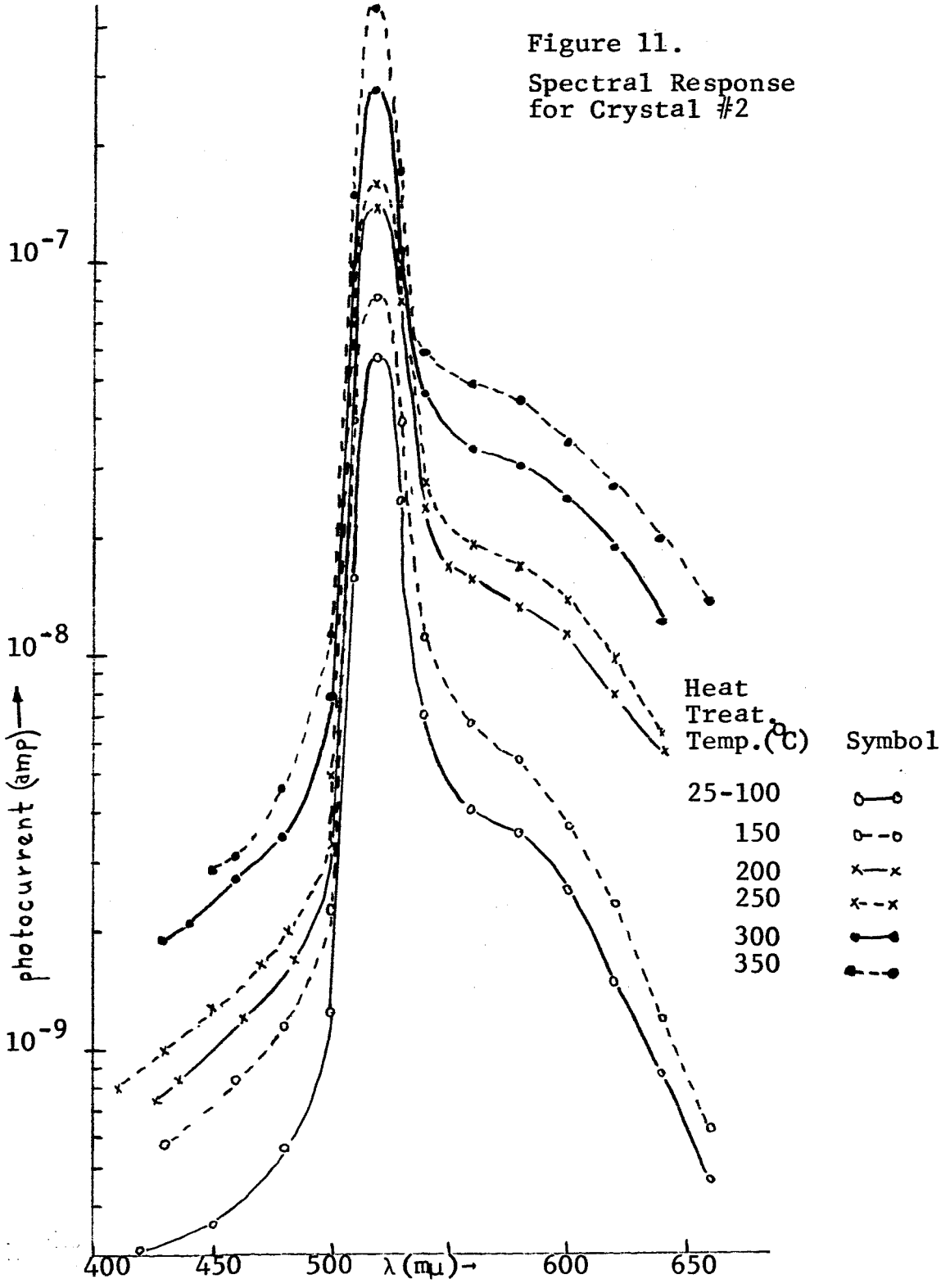
Figure 11.
Spectral Response
for Crystal #2
10^{-7}
10^{-8}
10^{-9}
photocurrent (amp)
400
450
500
λ(mμ)
600
650
Heat
Treat.
Temp.(°C)
Symbol
25-100
150
200
250
300
350

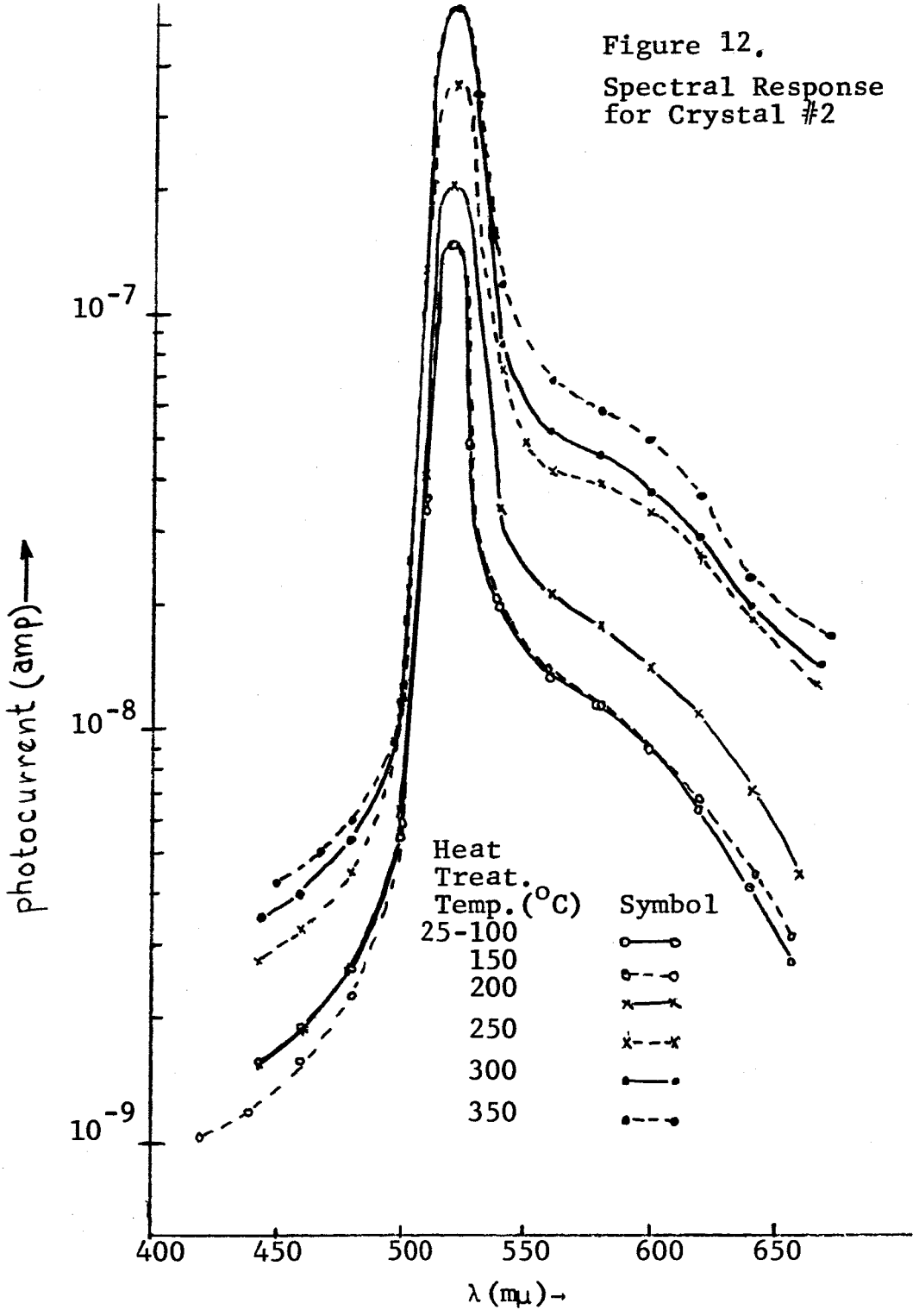

Figure 12.
Spectral Response for Crystal #2

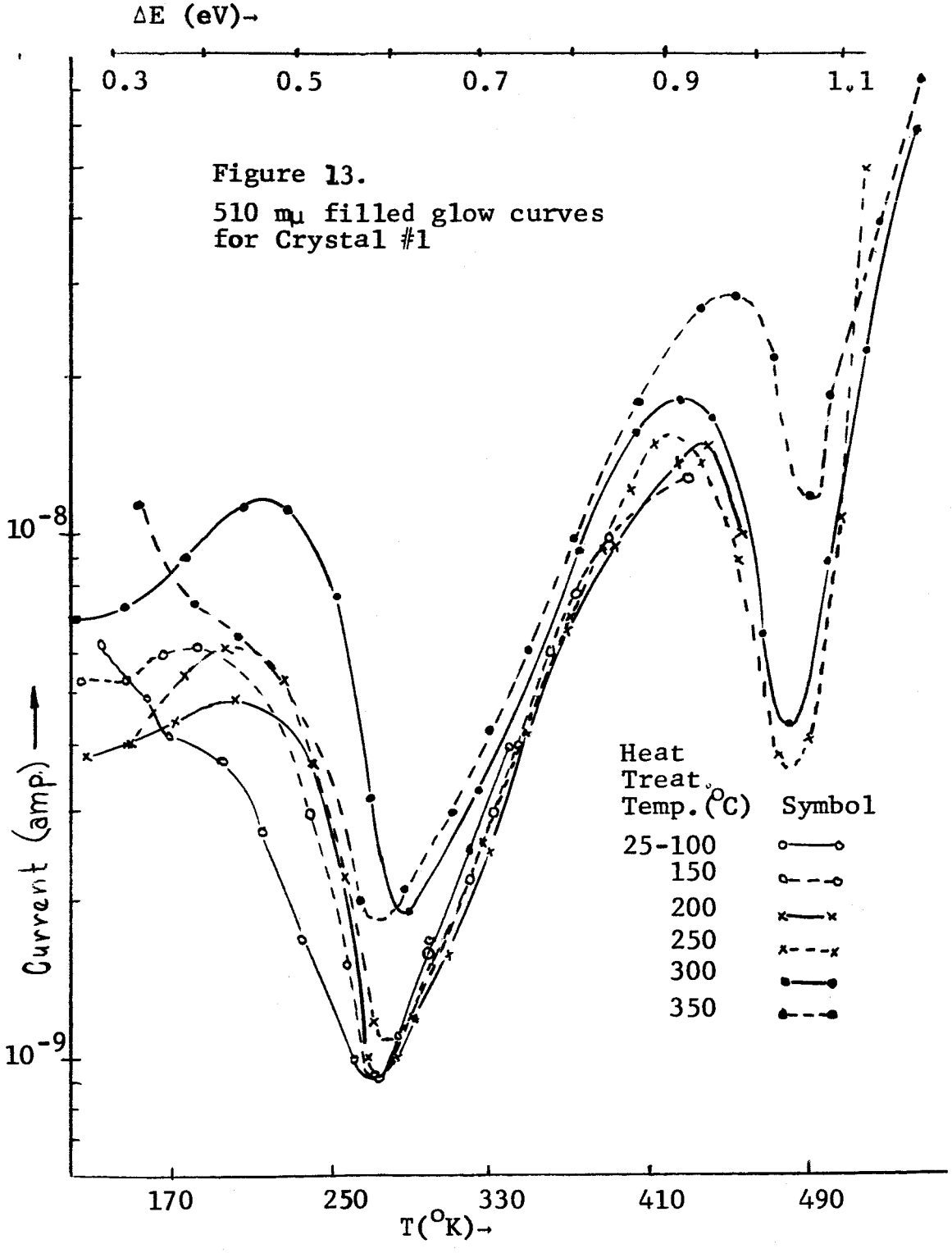
ΔE (eV)→
0.3
0.5
0.7
0.9
1.1
Figure 13.
510 mμ filled glow curves
for Crystal #1
10^{-8}
10^{-9}
Current (amp.) →
Heat
Treat.
Temp. (°C)
Symbol
25-100
150
200
250
300
350
170
250
330
410
490
T(°K)→

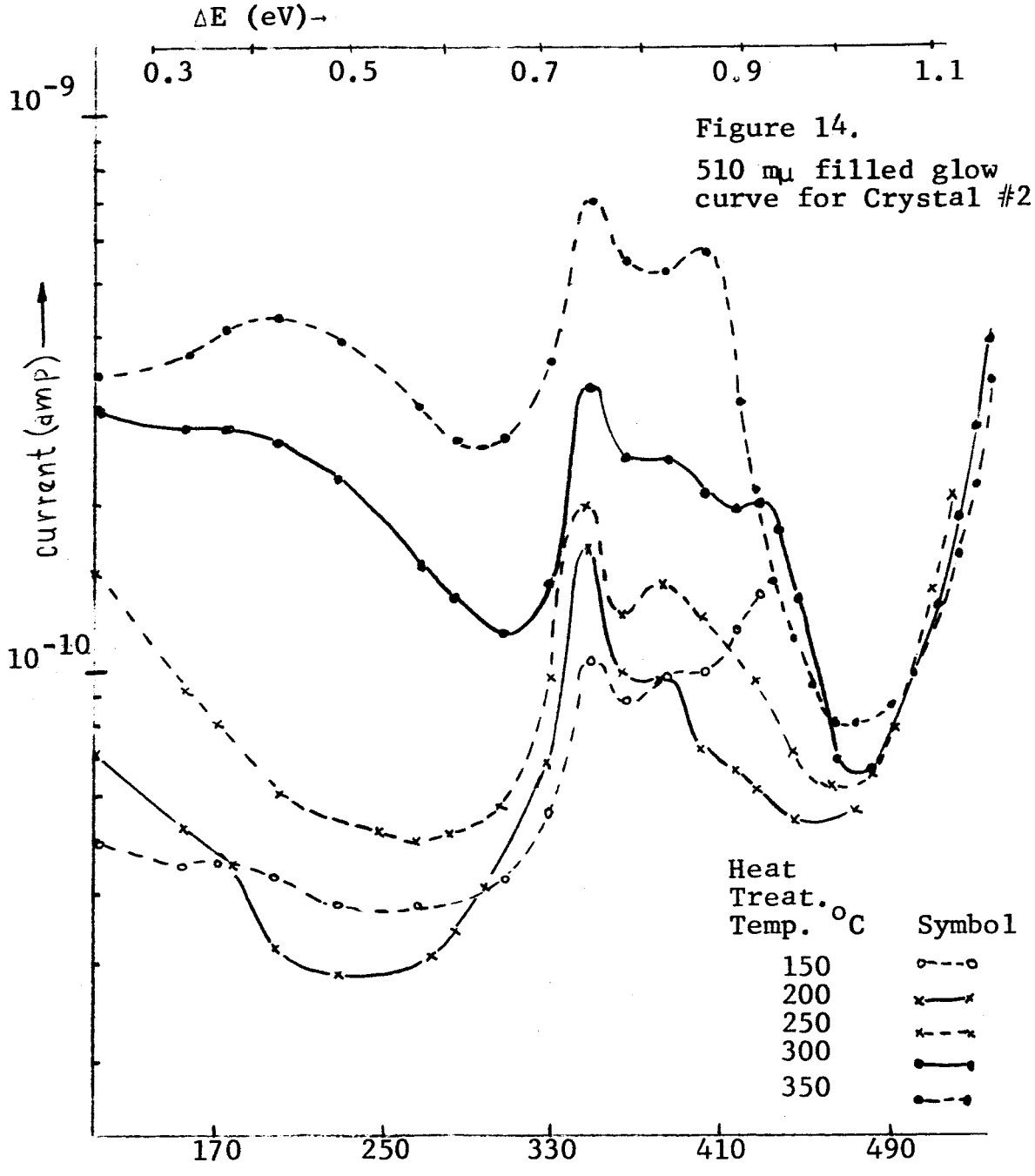

Figure 14.

510 mμ filled glow curve for Crystal #2

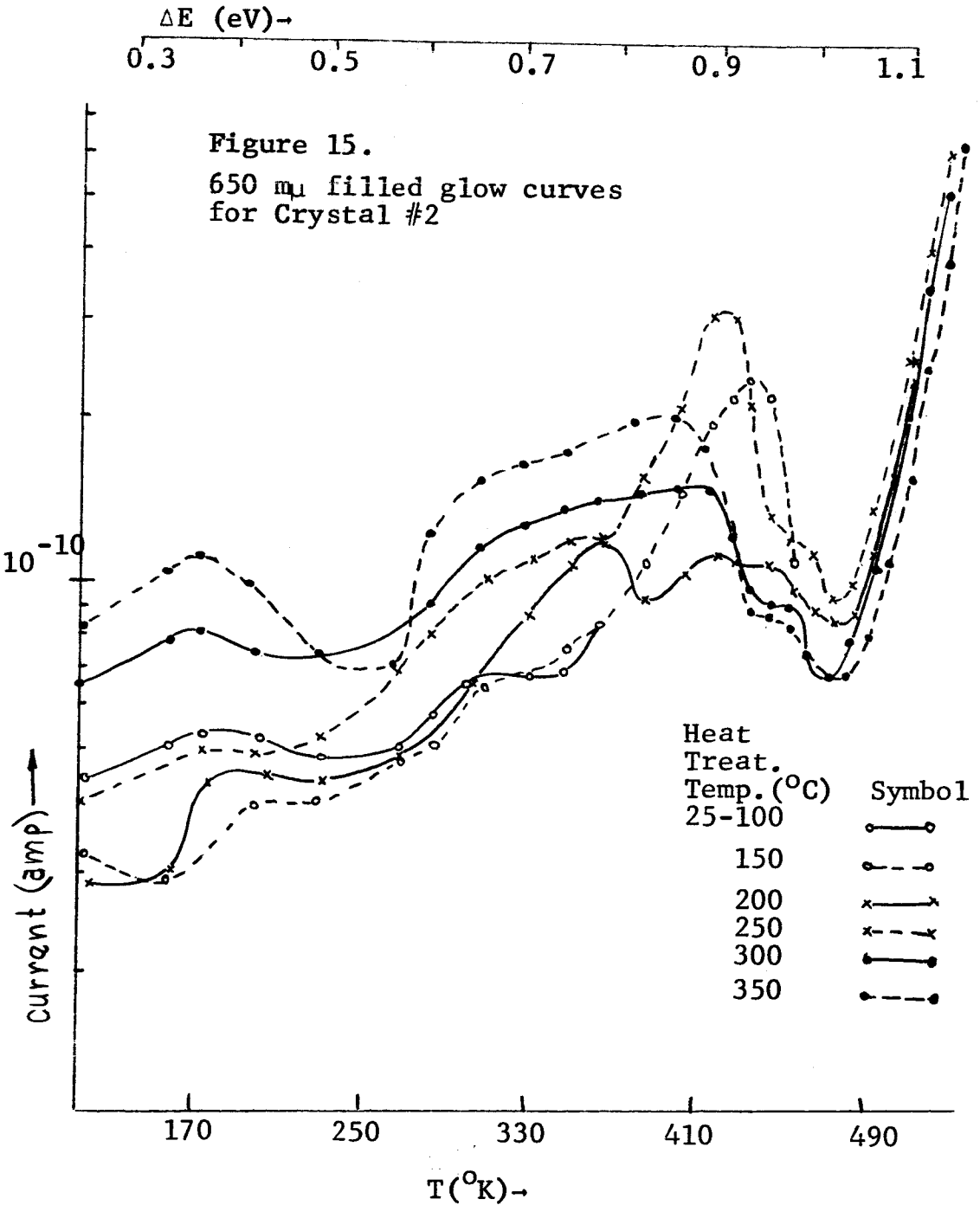

Figure 15.
650 mμ filled glow curves for Crystal #2

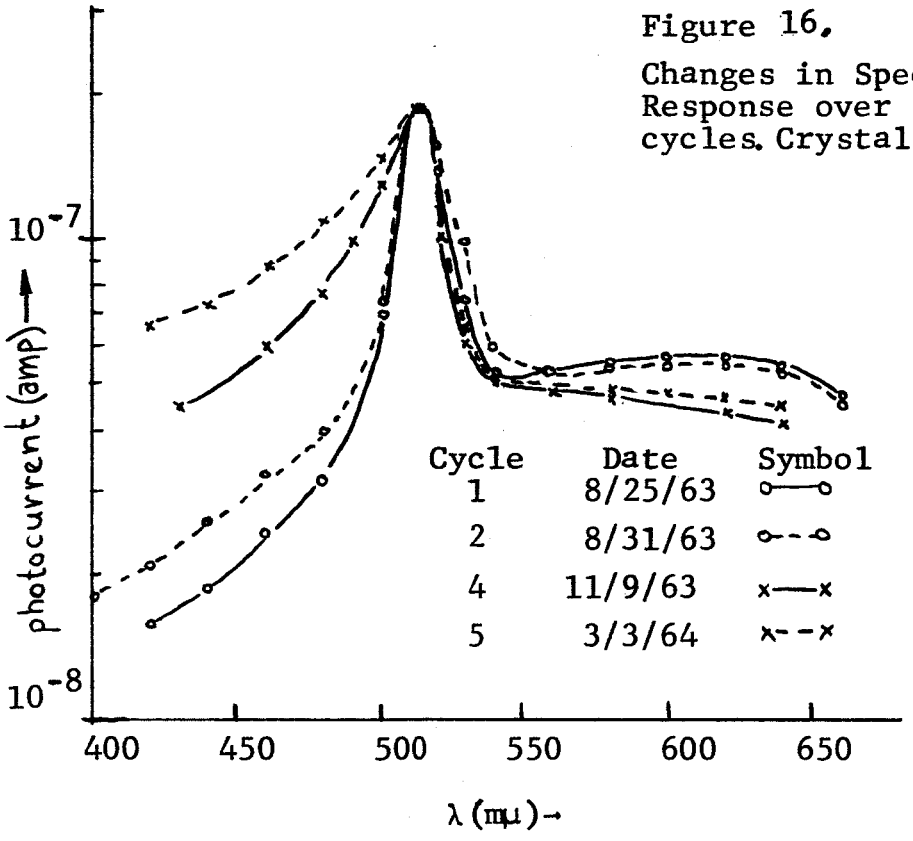

Figure 16.
Changes in Spectral Response over several cycles. Crystal #1

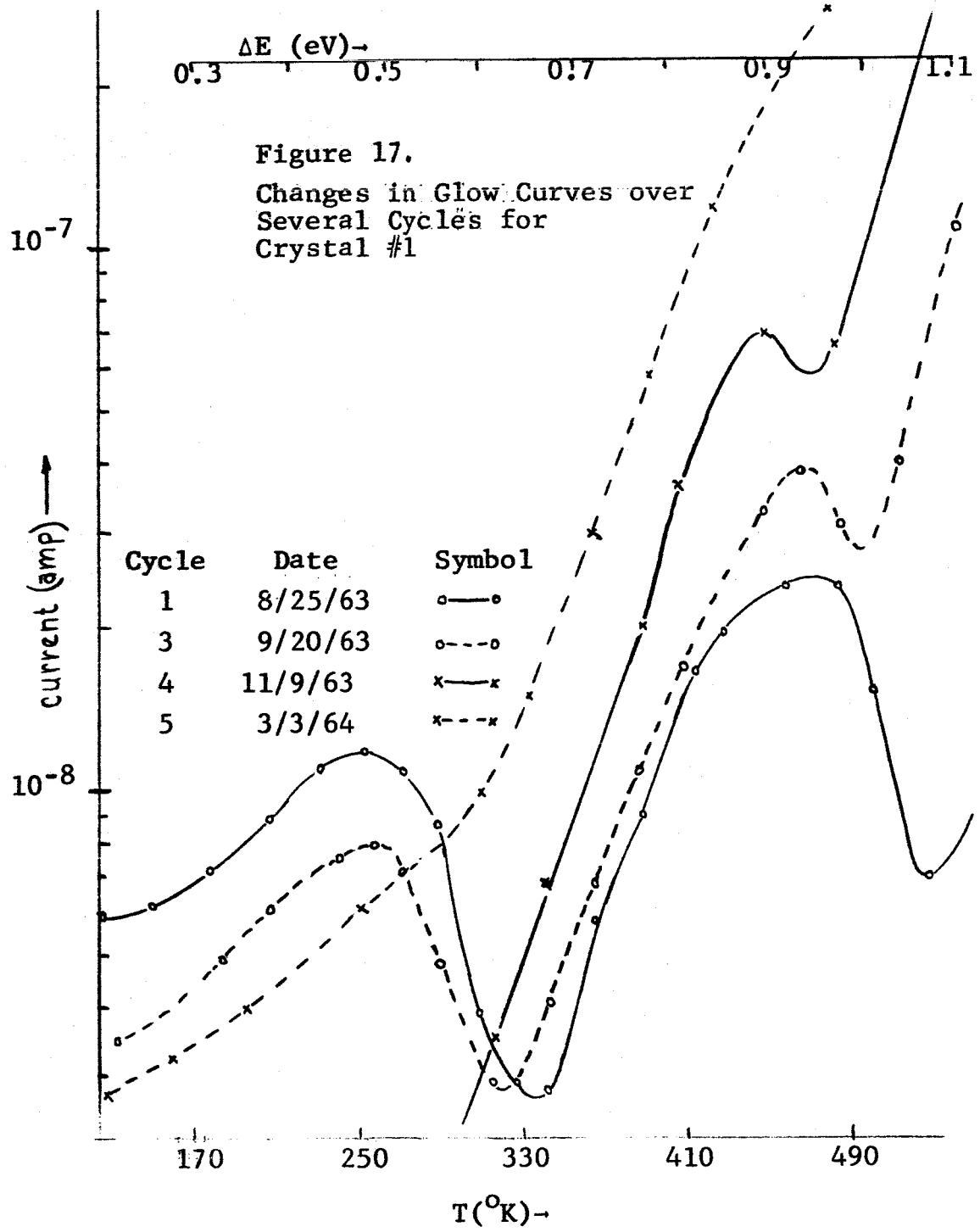

Figure 17.
Changes in Glow Curves over Several Cycles for Crystal #1

TABLE II

TRAP DENSITIES

The trap densities have been estimated using equation (C-11) derived in appendix C.

Figure 13

Heat Treat. Temp.	Glow Peak Temp. 200°K	440°K
100°C	1.0×10^{16}	--
200°C	1.5×10^{16}	6.4×10^{16}
300°C	2.9×10^{16}	6.3×10^{16}
350°C	1.6×10^{16}	9.0×10^{16}

Figure 14

Heat Treat. Temp.	Glow Peak Temp. 200°K	350°K	385°K	440°K
200°C	$<5\times10^{13}$	3×10^{14}	2×10^{14}	$<10^{13}$
250°C	$<5\times10^{13}$	2.4×10^{14}	2.4×10^{14}	$<10^{14}$
300°C	5×10^{14}	1.6×10^{14}	2.5×10^{14}	2×10^{14}
350°C	5×10^{14}	3.4×10^{14}		3.6×10^{14}

TABLE II (Contd.)

Figure 15

Heat Treat. Temp.	Glow Peak Temp. 180°K
100°C	-
200°C	-
300°C	6.4×10^{13}
350°C	1×10^{14}

Figure 17

Program	Glow Peak Temp. 250°K	450°K
1	3.3×10^{16}	5×10^{16}
3	1.7×10^{16}	1×10^{17}
4	$<10^{15}$	1.9×10^{17}
5	--	--

CHAPTER V

DISCUSSION OF RESULTS AND CONCLUSIONS

As was pointed out in Section II-3-1, the fact that the spectral response curves - specifically in the extrinsic range - suffer a wavelength independent increase in photocurrent with increasing heat treatment temperature requires that heat treatments result in an increase of the free carrier lifetime as opposed to an increase in the optical excitation rate. This is evident from the fact that a wavelength independent excitation rate requires a uniform increase in the entire level distribution over which the spectral response is examined. In addition, because this parallel shift occurs in crystals having markedly different extrinsic spectral responses, such a uniform increase in level distribution must also necessarily be independent of the level distribution. These restrictions render the suggested increase in optical excitation rate quite improbable thus insisting that heat treatments cause an increase in the free carrier lifetime.

In view of the arguments in section II-1, one expects that the effect of heat treatments, in the temperature range investigated here, is to dissociate defect associates, at least partially, thus giving rise to single point defects. The simplest model which can correlate the dissociation of associates with an increase in free carrier lifetime involves the destruction of associates which act as recombination centres. The reduction in the recombination centre density causes a decrease in the recombination rate thus increasing the steady state photocurrent. This can be seen by considering figure 4, Section II-3-2. If one assumes that recombination takes place primarily through one specie of centre

(via the γ transition), the steady state rate equation for conduction electrons becomes:

$$\frac{dn}{dt} = 0 = a - \gamma\, n(N_R - n_R) \qquad (21)$$

where a is the rate at which electrons are being excited into the conduction band per sec-cm^3 and $N_R - n_R$ is the density of recombination centres available for electron capture. Assuming for simplicity that most of the recombination centres are not occupied by electrons ($N_R \gg n_R$), the steady state electron concentration becomes:

$$n = \frac{a}{\gamma N_R} \qquad (22)$$

Hence the steady state photocurrent increases with decreasing N_R.

The fact that the increase in photocurrent is less in the intrinsic range than it is in the extrinsic range for heat treatments up to 300°C for crystal #1 and up to 350°C for crystal #2 is explainable in terms of a higher density of recombination centres in the near surface region than in the bulk of the crystal. If, for instance, the effect of heat treatments is to destroy a certain density of some specie of recombination centre essentially uniformly throughout the crystal and if the density of recombination centres were somewhat larger in the near surface region - as one might expect (c.f. sections II-2 and II-3-1) both from the spreading of the quasi-Fermi levels (due to the high intrinsic absorption) and from the presence of many surface imperfections - the resulting rise in intrinsic photocurrent would be smaller because the percent reduction of recombination centres per cm^3 would be less near the surface than in the bulk.

The TSC peaks at approximately 200°K (~0.4 eV) and 440°K (~0.95 eV) which grow to concentrations of ~ 5 x 10^{14} cm^{-3}(Figure 14) can be associated with the products of the dissociated recombination centres where, by the arguments in Section II-1-4, at least one of these peaks is due to a single intrinsic point defect and the other either a different single point defect or a residual subcluster. This then suggests that the primary recombination mechanism in crystal #2 is due to a defect associate whose density, by equation 21, is probably on the order of 10^{15} cm^{-3} since the dissociation of approximately 10^{14} cm^{-3} results in a current change of the order of 10%. If one assumes that the same associate was responsible.

For recombination in both crystals #1 and #2 then, since the photoconductivities of both crystals were nearly the same (as can be seen by comparing figures (10-12)), the recombination centre densities must have been nearly equal. This can then explain two features of the behavior of crystal #1. First, that the peaks at 200°K and 440°K exhibited no appreciable growth per cycle in crystal #1 is due to the fact that 10^{14} additional traps of these types per cm^3 would go unnoticed in a background concentration in excess of 10^{16}. Second, that the parallel shifts with increasing heat treatment temperatures were less in crystal #1 than in crystal #2 is due to the fact that the large background densities of the products of dissociation (viz. defects giving rise to the 200°K and 440°K peaks) would impede dissociation of the defects as can be seen from the mass-action arguments in section II-1-4 (equation 13). As mentioned in section IV-2-2, experiments currently underway have shown that crystals heat treated in sulfur vapor exhibit TSC curves consisting almost entirely of a pronounced peak at 440°K (>$10^{17}cm^{-3}$) with the peak at 200°K absent. When subjected to heat treatment-annealing cycles of

the type described in this thesis, the parallel shifts in photoconductivity were, although present, quite small (<10% from 100°C to 350°C heat treatments) while the photoconductivities (i.e. spectral response curves) were less than half an order of magnetude lower than those of crystals #1 or #2. This behavior is in agreement with the above proposed explanation since a large concentration of the 440°K peak defect, by the above arguments would impede dissociation and may force a slightly higher associate concentration.

An interesting outcome of the behavior of crystal #1 stems from the fact that although both the 200°K and the 440°K peak defects were quite abundant in this crystal, the recombination traffic was no greater than for crystal #2. Since the concentration of each of these defects was two orders of magnitude higher in crystal #1 than in crystal #2, one expects from the mass-action arguments in section II-1-4 (equation 11) that, if only these two defects were needed to form the recombination centre, the resultant equilibrium concentration of associates in crystal #1 should be four orders of magnitude higher than in crystal #2. Since this appears not to be the case, one is led to conclude that the associate responsible for recombination is composed of at least a third member - which in this experiment is undetected - and hence the abundance of these recombination centres is limited by the abundance of this third member.

A lower bound of the electron capture cross section of the recombination associate can be obtained. From the steady state rate equation (equation 21),

$$S_n = \frac{a}{n\bar{v}_{th}(N_R - n_R)} = \frac{1}{\tau \bar{v}_{th}(N_R - n_R} \qquad (23)$$

Using the values $\tau \simeq 10^{-3}$sec. (equation C-7), $V_{th} \simeq 3 \times 10^{7}$ cm/sec (equation B-2) and $N_R - n_R \simeq 10^{15}$ cm^{-3} one obtains:

$$S_n \simeq 10^{-20} \text{ cm}^2$$

A TSC peak at approximately 180°K has been identified by several authors (5, 13, 14) as being due to a cadmium vacancy on the basis that it appears when the crystals have been heat treated in atmospheres of sulfur, oxygen or gallium and disappears upon heat treating in cadmium or vacuo. Since the broad 200°K peak obtained in this investigation lies in the same energy range and also exhibits the property of disappearing after heat treatments in vacuo (Section IV-2-2), it seems reasonable to assume that the defect responsible for this peak is also the cadmium vacancy.

Simultaneous with the irreversible decrease of the 200°K TSC peak is the increase in surface photocurrent and dark current. It is well known that the presence of oxygen on the crystal's surface causes a decrease in the photoconductivity (55,56) and the dark conductivity (57) and that baking the crystal in an oxygen atmosphere can give rise to a TSC peak at 180°K (5,13). Conversely then, one expects that, if desorption of adsorbed oxygen layers is present, one should observe a decrease in the V_{cd} concentration and an increase in the intrinsic spectral response and dark current. Since, in an "ion-pumped" system ($\sim 10^{-10}$ torr) which has been fore-pumped with a vac-sorb pump, the largest partial pressures are those of hydrogen and helium - with oxygen accounting for less than 10% of the residual atmosphere-(58), it is possible that some replacement mechanism is in operation whereby desorbed oxygen is replaced, for example, by hydrogen - which has been shown to have little effect on the spectral distribution of photoconductivity of CdS (55).

Due to the fact that all of the five sulfur treated crystals thus far investigated exhibit pronounced TSC peaks at 440°K, one is required to assign to this peak a defect involving the cadmium vacancy - perhaps corresponding to some higher order S_n - molecule. That this peak grew irreversibly upon 350°C heat treatments might also be connected with the depletion of the 200°K V_{cd} peak by reasoning that, at 350°C, the cadmium vacancies have enough thermal energy to overcome their mutual ionic repulsion and hence to associate thus forming additional 440°K peak defects. These S_n clusters however are tightly bound at 350°C and hence one notices a decrease in their number (i.e. during annealing) only when the V_{cd} and the undetected third member associate with them to form recombination centres.

The difference between the peak structures of the glow curves filled with 510 mμ light (figure 14) and those filled with 650 mμ light (figure 15) in crystal #2 - viz. the appearance of peaks at 350°K and 385°K in figure 14 - is not presently explainable. A possible explanation is that these traps have small capture cross-sections and hence require a long time (longer than 50 minutes) at the lower electron densities afforded by weakly absorbed 650 mμ light to become noticibly full. Another possibility is that of the presence of the so-called photochemical reactions (59-62). These are believed to occur even at room temperature (62). Experiments to investigate the dependence of trap filling on wavelength are presently being planned.

LITERATURE CITED

1. W. Veith, Z. angew. Physik, 7, 1 (1955).
2. A. C. Aten, J. H. Haanstra and H. de Vries, Philips Res. Repts., 20, 395-403, (1965).
3. B. A. Kulp, K.A. Gale and R. G. Schulze, Phys. Rev. vol. 140 A252-6 (1965).
4. R. H. Bube, Phys. Rev., 99, 1105 (1955).
5. J. Woods, J. Electron Control, vol. 5, pp. 417-26, (1958).
6. F. A. Kroger, H. J. Vink and J. Van den Boomgaard, Z. Phys. Chem. 203, 1 (1954).
7. K. H. Nicholas and J. Woods, Brit. J. Of Appl. Phys., vol. 15, pp. 783-95, (1964).
8. U. Buget and G. T. Wright, Brit. J. Appl. Phys. 16, pp. 1457-60 (1965).
9. B. A. Kulp and R. H. Kelley, J. Appl. Phys. 31, 1057-61, (1960).
10. B. A. Kulp, J. Appl. Phys. 32, 1966-9, (1961).
11. K. W. Boer, E. H. Weber and B. Wojtowicz, Z. Phys., 168, pp. 115-28, (1962).
12. K. W. Boer, J. C. O'Connell and R. Schubert, Int. Conf. Lumines., Munich, Verl. Karl Thiemigs, p. 375, (1965).
13. J. S. Skarman, Solid-State Electronics, vol. 8, pp. 17-29, (1965).
14. J. Woods and D. A. Wright, Sol. State Phys. in Elect. and Telecomm., 2, Part 2, p. 880, (Brussels Conference) (1958).
15. A. P. Trofimenko, G. A. Fedorus, and A. K. Razmadze, Sov. Phys.-Sol. State vol 2, pp. 1033-8, (1960).
16. R. Boyn, O. Goede, and S. Kuschnerus, Phys. State Sol. 12, 57-70, (1965).
17. H. H. Woodbury, Phys. Rev. Vol. 134, pp. A492-8, (1964).
18. E. A. Niekisch, Z. fur Phys. Chem. (Leipzig) vol. 216, pp. 110-135.
19. C. Kittel, Introduction to Solid State Physics, John Wiley and Sons, Inc., New York, Chapter 13.

20. F. A. Kroger, The Chemistry of Imperfect Crystals, John Wiley and Sons, Inc., New York, Chapter 13.

21. D. Berlincourt, H. Jaffe and R. Shiozawa, Phys. Rev. Vol. 129, pp. 1009-17, (1963).

22. C. Kittel, Introduction to Solid State Physics, John Wiley and Sons, Inc., New York, Chapter 17.

23. N. F. Mott and R. W. Gurney, Electronic Processes in Ionic Crystals (second edition), Dover Publications, Inc., pp. 29-32.

24. K. W. Boer, R. Boyn, and O. Goede, Phys. Stat. Sol. vol. 3, pp. 1684-94, (1963).

25. W. W. Anderson, App. Phys. Letters, vol. 7, No. 7, pp. 198-200, (1965).

26. K. W. Boer, H. Hornung and K. L. Zimmermann, Monatsber, DAW, vol. 2, pp. 159-61, (1960).

27. F. E. Williams, J. Phys. Chem. Solids, Vol. 12, pp. 265-75, (1960).

28. E. F. Apple and F. E. Williams, J. Electrochem. Soc. vol. 106, pp. 224-230, (1959).

29. F. A. Kroger, The Chemistry of Imperfect Crystals, John Wiley and Sons, Inc., New York, Chapter 9.

30. F. A. Kroger, Ibid., p. 297.

31. S. Arrhenius, Z. Phys., 82, 716, (1933). This has also been confirmed by L. Brewer and R. E. Honig (private communication).

32. C. Kittel, Introduction to Solid State Physics, 2nd Ed., John Wiley and Sons, New York, p. 99.

33. R. A. Smith, Wave Mechanics of Crystalline Solids, Chapman and Hall, Ltd. London, pp. 298-302.

34. R. H. Bube, Photoconductivity of Solids, John Wiley and Sons, Inc., pp. 273-324.

35. A. Rose, Concepts in Photoconductivity and Allied Problems, John Wiley and Sons, Inc., Chapter 3.

36. I. Tamm, Physik Z. Sowjetunion, vol. 1, 733, (1932).

37. J. Bardeen, Phys. Rev. 71; 717 (1947).

38. D. Dutton, Phys. Rev., vol. 112, No. 3, 785-92, (1958).

39. K. W. Boer, S. Oberlander and J. Voigt, Ann. Der Physik. vol. 7, 136 (1958).

40. J. T. Randall and M. H. F. Wilkins, Proc. Roy. Soc. A, vol. 184, 365, (1945).

41. A. Bohun, Czech J. Phys., vol. 4, 91 (1954).

42. A. H. Booth, Canad. J. Chem., vol. 32, 214 (1954).

43. R. H. Bube, J. Chem. Phys., Vol. 23, 18 (1955).

44. G. F. J. Garlick and A. F. Gibson, Proc. Phys. Soc., vol. 60, 574, (1960).

45. L. I. Grossweiner, J. Appl. Phys., vol. 24, 1306 (1953).

46. R. R. Haering and E. N. Adams, Phys. Rev., vol. 117, 451 (1960).

47. A. Halperin and A. A. Braner, Phys. Rev. vol. 117, 408, (1960).

48. P. N. Keating, Proc. Phys. Soc., vol. 78, 1408, (1961).

49. Ch. B. Luschik, Dok. Akad, Nauk. USSR,, vol. 101, 641, (1955).

50. M. Schon, Tech.-Wiss. Abh. Osrom-Ges. vol. 7, 175 (1958).

51. H. J. Dittfeld and J. Voigt, Phys. Stat. Sol. vol. 3, 1941, (1963).

52. R. H. Bube, Photoconductivity of Solids, John Wiley and Sons, Inc., New York, p. 295.

53. E. Spenke, Electronic Semiconductors, McGraw-Hill Book Company, Inc., Chapter IV.

54. K. W. Böer and W. Borchardt, Fortschr. d. Physik, vol. 1, pp. 184-6, (1953).

55. H. Berger, K. W. Böer and E. H. Weber, Zeit. Phys. vol. 158, 501-510, (1960).

56. G. Kuwabara, J. Phys. Soc. Japan Vol. 9, No. 1, pp. 97-102, (1954).

57. W. Muscheid, Ann. der Physik., 6 Folge., Band 13, (1953).

58. R. Schubert (private communication).

59. K. W. Böer, Physics vol. 20, 1103, (1954).

60. K. W. Böer, E. Borchardt and W. Borchardt, Arbeitstagung Festkorperphysik, Dresden, pp. 12-17, (1954).

61. K. W. Böer, W. Borchardt and S. Oberlander, Zeit. fur Phys. Chem., vol. 210, pp. 218-31, (1959).

62. J. Woods and K. H. Nicholas, Brit. J. Appl. Phys., vol. 15, 1361-7 (1964).

63. A. Addamiano, J. Phys. Colloid Chem., Vol. 61, 1253, (1957)

64. A. H. Cottrell, The Mechanical Properties of Matter, John Wiley and Sons, Inc., New York, p. 70.

65. R. Groth and M. Memming, Phys. Stat. Sol., Vol. 1, 650, (1961).

66. E. Spenke, Electronic Semiconductors, McGraw-Hill Book Company, Inc., Chapter VII.

67. R. Seiwert, Ann. Phys., Vol. 6, 241, (1949).

68. R. H. Bube, J. Appl. Phys. Vol. 34, No. 11, 3309-14, (1963).

69. Cleaning Procedures for Ultra High Vacuum Systems-Varian Associates.

APPENDIX A

An estimate of the upper bound on the equilibrium concentration of Schottky defects in CdS at 350°C can be obtained for CdS by considering the melting point: 1748°K (63).

Cottrell (64) suggests that at the melting point the degree of disorder is

$$\frac{n}{N_L} \approx 10^{-4}. \qquad \text{(A-1)}$$

Allowing the degree of disorder to be even as high as 10^{-2} and using the lowest proposed value (23) for γ_s (i.e. 10^3) one obtains:

$$\frac{n}{N_L} = 10^{-2} = 10^3 \, e^{-\frac{E_s}{0.3}} \qquad \text{(A-2)}$$

or

$$E_s = 3.45 \text{ eV} \qquad \text{(A-3)}$$

Figure 18 is a plot of equilibrium defect concentration versus formation energy for T = 350°C and $\gamma_s = 10^3$. It is seen from this figure that for a formation energy of 3.5 eV the concentration of Schottky defects is $10^{11} cm^{-3}$. In view of the fact that the changes in defect structure observed in this investigation (viz. growth of peaks in TSC curves) involve concentrations in excess of 10^{14} cm^{-1}, it is improbable that the Schottky mechanism is responsible for these defects.

Since the factor γ_f for Frenkel defects is believed to be less than 10^3 (see Section II-1-2) the concentration of Frenkel defects corresponding to any given energy of

formation is less than the concentration of Schottky defects.

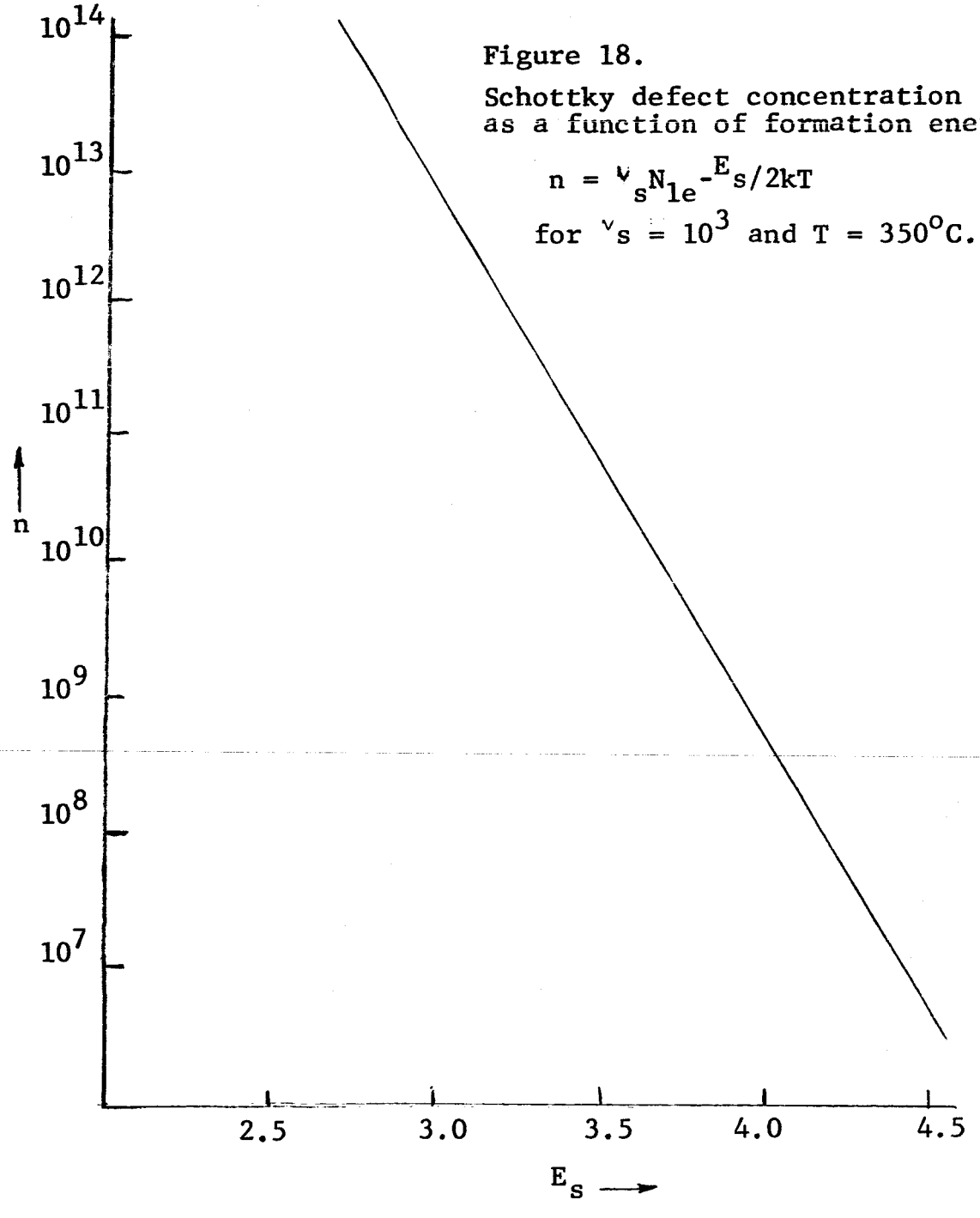

Figure 18.
Schottky defect concentration as a function of formation energy

$n = \nu_s N_{1e}^{-E_s/2kT}$

for $\nu_s = 10^3$ and $T = 350^{\circ}C$.

APPENDIX B

The mean free path L between collisions with imperfections and phonons for an electron traveling through a crystal with thermal velocity V_{th} can be obtained from the product of the thermal velocity and the collision time T_c.

The thermal velocity is obtained from the relation.

$$\frac{1}{2} M^* V_{th} = \frac{3}{2} kT \qquad \text{(B-1)}$$

where M* is the effective mass of the electron (=0.2 m_o(65)). Hence, at room temperature, for CdS,

$$V_{th} = 2.6 \times 10^7 \text{ cm/sec.} \qquad \text{(B-2)}$$

The collision time T_c can be obtained from the mobility and the effective mass through the relation (66);

$$\mu = \frac{eT_c}{2M^*} \qquad \text{(B-3)}$$

The mobility μ for CdS at room temperature is 200 cm^2/V-sec (67). Hence,

$$T_c \sim 4 \times 10^{-14} \text{sec.} \qquad \text{(B-4)}$$

Hence the mean free path is;

$$L \sim 10^{-6} \text{ cm.} \qquad \text{(B-5)}$$

APPENDIX C

From the area beneath a glow peak one can estimate the density of the level in the following way. If the electrons freed from the trapping level were permitted to travel the length of the crystal before recombining, the number of electrons liberated from the trap would be given by:

$$N' = \frac{i_{(t)}dt}{e} \qquad \text{(C-1)}$$

where $i_{(t)}$ is the current of the glow curve as a function of time. However, because the electrons do recombine after having spent a lifetime in the conduction band T (which is different from the drift time required for an electron to travel the length of the crystal T_D) it is clear that the number of electrons contributing to the peak is:

$$N = \frac{i_{(t)}dt}{e(T/TD)} \qquad \text{(C-2)}$$

The ratio T/TD is called the photoconductive gain.

The times T and T_D can be estimated from the accompanying spectral response curve, if we neglect their temperature and light intensity dependence,(68) in the following manner.

The electron lifetime T can be obtained from the steady state equation:

$$n = aT \qquad \text{(C-3)}$$

where n is the conduction electron concentration and a is the rate at which electrons are being optically excited into

the conduction band per cm^3 (assumed equal to the rate per cm^3 of photon absorption). n can be found from the spectral response curve from the expression.

$$i = ne_{\mu}EA \qquad \text{(C-4)}$$

where e is the electronic charge, the mobility, E electric field and A the area of the crystal perpendicular to the direction of current flow.

The quanity a can be found from Figure 8 curve #2. At 515 m_{μ} 80% of the incident light is absorbed. Hence, at 515 m_{μ}

$$a \sim \frac{0.8}{(Th)} \times 10^{13} \text{ electrons / } cm^3\text{-sec.} \qquad \text{(C-5)}$$

where (Th) is the thickness of the crystal ($\sim 5 \times 10^{-3}$ cm.). Hence:

$$a \sim 1.6 \times 10^{15} \text{ electrons / } cm^3\text{-sec.} \qquad \text{(C-6)}$$

Combining equations (C-3), (C-4) and (C-6) we obtain

$$T \sim \frac{i}{e_{\mu}EA(1.6)} \times 10^{-15} \text{ sec.} \sim 10^{-3} \text{sec.} \qquad \text{(C-7)}$$

where i is the current at 515 m_{μ}. The drift time T_D is given by:

$$T_D = \frac{L}{V_D} = \frac{L}{\mu E} \qquad \text{(C-8)}$$

where L is the length of the crystal.

Hence combining (C-7) and (C-8) we obtain

$$T/T_D \sim \frac{i \quad x\ 10^{-15}}{eV\ (1.6)} \qquad \text{(C-9)}$$

where V is the volume of the crystal. Substituting (C-9) into (C-2) we obtain:

$$\frac{N}{V} = \frac{\int i(t)dt}{i} \, 1.6 \times 10^{15} \qquad \text{(C-10)}$$

Approximately the integral $\int i(t)dt$ by $i_{max} \Delta t$, where Δt is the half width of the glow peak ($\Delta t = \frac{\Delta T}{\text{(heating rate)}}$) and i_{max} is the current at the maximum, we obtain for the number of electrons liberated per cm^3.

$$n_{tr} = \frac{i_{max} \ \Delta T}{i} \ 5 \times 10^{15} \qquad \text{(C-11)}$$

If we assume that the traps were filled initially, equation (C-11) gives us the density of trapping levels located at an energy 25 kT_m below the Conduction band.

APPENDIX D

Varian Associates recommends the following procedures for cleaning stainless steel (69).

1. Solvent degrease - Trichloroethylene or equivalent. Three stages, liquid dip, vapor, drain and dry.
2. Hot alkali dip - Approximately 2 minutes depending on condition.
3. Hot tap water rinse.
4. Hydrochloric acid dip - (Solution 1:1 HCl (Tech) in water at 70°C).
5. Cold tap water rinse.
6. Nitric - Hydrofluoric acid dip - 97 volume % conc. HNO_3 3 volume % conc. HF. Dip until surface gases slightly. Increase rate of attack. Handle with all caution and respect due hydrofluoric acid.
7. Cold tap water rinse - Repeat twice.
8. Deionized water rinse, cold (NaCl less than 1 p.p.m.) Repeat twice.
9. Methanol rinse - Use electronic grade.
10. Warm air dry - In clean, filtered, fume-free air at approximately 65°C.